



THE UNIVERSITY *of* EDINBURGH

Edinburgh Research Explorer

ZC3H4 restricts non-coding transcription in human cells

Citation for published version:

Estell, C, Davidson, L, Steketee, PC, Monier, A & West, S 2021, 'ZC3H4 restricts non-coding transcription in human cells', *eLIFE*, vol. 10, 2021;10:e67305. <https://doi.org/10.7554/eLife.67305>

Digital Object Identifier (DOI):

[10.7554/eLife.67305](https://doi.org/10.7554/eLife.67305)

Link:

[Link to publication record in Edinburgh Research Explorer](#)

Document Version:

Publisher's PDF, also known as Version of record

Published In:

eLIFE

General rights

Copyright for the publications made accessible via the Edinburgh Research Explorer is retained by the author(s) and / or other copyright owners and it is a condition of accessing these publications that users recognise and abide by the legal requirements associated with these rights.

Take down policy

The University of Edinburgh has made every reasonable effort to ensure that Edinburgh Research Explorer content complies with UK legislation. If you believe that the public display of this file breaches copyright please contact openaccess@ed.ac.uk providing details, and we will remove access to the work immediately and investigate your claim.



1 **ZC3H4 restricts non-coding transcription in human cells**

2

3

4 Chris Estell¹, Lee Davidson¹, Pieter C. Steketee², Adam Monier¹ and Steven West^{1*}

5

6

7 ¹The Living Systems Institute, University of Exeter, Stocker Rd, Exeter, EX4 4QD

8 ² The Roslin Institute, Royal (Dick) School of Veterinary Studies, University of Edinburgh,
9 Edinburgh, EH25 9RG

10

11

12 *Lead contact: s.west@exeter.ac.uk; telephone 0044(0)1392727458

13

14

15

16 Keywords: ZC3H4; Transcription termination; enhancer; non-coding RNA; super-enhancer;
17 exosome; antisense; RNA polymerase II; Integrator

18

19

20

21

22

23

24

25

26

27 **SUMMARY**

28 The human genome encodes thousands of non-coding RNAs. Many of these terminate
29 early and are then rapidly degraded, but how their transcription is restricted is poorly
30 understood. In a screen for protein-coding gene transcriptional termination factors, we
31 identified ZC3H4. Its depletion causes upregulation and extension of hundreds of unstable
32 transcripts, particularly antisense RNAs and those transcribed from so-called super-
33 enhancers. These loci are occupied by ZC3H4, suggesting that it directly functions in their
34 transcription. Consistently, engineered tethering of ZC3H4 to reporter RNA promotes its
35 degradation by the exosome. ZC3H4 is predominantly metazoan - interesting when
36 considering its impact on enhancer RNAs that are less prominent in single-celled organisms.
37 Finally, ZC3H4 loss causes a substantial reduction in cell proliferation, highlighting its overall
38 importance. In summary, we identify ZC3H4 as playing an important role in restricting non-
39 coding transcription in multi-cellular organisms.

40

41

42

43

44

45

46

47

48

49

50

51

52

53

54

55

56 INTRODUCTION

57 Most of the human genome can be transcribed by RNA polymerase II (Pol II).
58 Among these transcripts are thousands of long non-coding RNAs, broadly classified as
59 greater than ~200 nucleotides in length (Kopp and Mendell, 2018). They share some
60 structural features with coding transcripts, but most of them are rapidly degraded by the
61 exosome (Davidson et al., 2019; Preker et al., 2008; Schlackow et al., 2017). Their
62 degradation is coincident with or shortly after transcriptional termination, which often occurs
63 within a few kilobases (kb). The mechanisms for terminating non-coding transcription are
64 poorly understood, especially by comparison with those operating at protein-coding genes.

65 Termination of protein-coding transcription is coupled to 3' end processing of pre-
66 mRNA via cleavage at the polyadenylation signal (PAS) (Eaton and West, 2020). A PAS
67 consists of an AAUAAA hexamer followed by a U/GU-rich region (Proudfoot, 2011). After
68 assembly of a multi-protein processing complex, CPSF73 cleaves the nascent RNA and the
69 Pol II-associated product is degraded 5'→3' by XRN2 to promote termination (Eaton et al.,
70 2018; Eaton et al., 2020; Fong et al., 2015). The Pol II elongation complex is modified as it
71 crosses the PAS, which facilitates its termination by XRN2 (Cortazar et al., 2019; Eaton et
72 al., 2020). Depletion of XRN2 or CPSF73 causes read-through downstream of some long
73 non-coding genes (Eaton et al., 2020). However, a substantial fraction of non-coding
74 transcription is less sensitive to their depletion suggesting the use of alternative
75 mechanisms.

76 The Integrator complex aids termination of many non-coding transcripts, with the
77 archetypal example being snRNAs (Baillat et al., 2005; Davidson et al., 2020; O'Reilly et al.,
78 2014). Integrator is also implicated in the termination of promoter upstream transcripts
79 (PROMPTs) and enhancer RNAs (eRNAs) (Beckedorff et al., 2020; Lai et al., 2015; Nojima
80 et al., 2018). The mechanism is analogous to that at protein-coding genes, driven by
81 endonucleolytic cleavage by INTS11. However, INTS11 activity does not precede XRN2
82 degradation at snRNA genes (Eaton et al., 2018). Moreover, while CPSF73 is indispensable
83 for termination at protein-coding genes, there is evidence of redundant pathways at snRNA
84 loci (Davidson et al., 2020). Indeed, CPSF and the cap binding complex-associated factor,
85 ARS2, are both implicated in the termination of promoter-proximal transcription (Iasillo et al.,
86 2017; Nojima et al., 2015).

87 A variety of processes attenuate transcription at protein-coding genes (Kamieniarz-
88 Gdula and Proudfoot, 2019). Frequently, this is via premature cleavage and polyadenylation
89 (PCPA) that can be controlled by U1 snRNA, CDK12, SCAF4/8 or PCF11 (Dubbury et al.,
90 2018; Gregersen et al., 2019; Kaida et al., 2010; Kamieniarz-Gdula et al., 2019). PCPA is

91 common on many genes since acute depletion of the exosome stabilises its predicted
92 products in otherwise unmodified cells (Chiu et al., 2018; Davidson et al., 2019). Integrator
93 activity also attenuates transcription at hundreds of protein-coding genes.

94 A less-studied termination pathway at some intragenic non-coding regions is
95 controlled by WDR82 and its associated factors (Austena et al., 2015). In mammals,
96 WDR82 forms at least two complexes: one with the SETD1 histone methyl-transferase and
97 another composed of protein-phosphatase 1 and its nuclear targeting subunit PNUTS (Lee
98 et al., 2010; van Nuland et al., 2013). A version of the latter promotes transcriptional
99 termination in trypanosomes (Kieft et al., 2020) and the budding yeast homologue of
100 WDR82, Swd2, forms part of the APT (associated with Pta1) termination complex (Nede et
101 al., 2003). In murine cells, depletion of either WDR82, PNUTS or SET1 causes non-coding
102 transcriptional termination defects (Austena et al., 2015). Notably, PNUTS/PP1 is
103 implicated in the canonical termination pathway at protein-coding genes where its
104 dephosphorylation of SPT5 causes deceleration of Pol II beyond the PAS (Cortazar et al.,
105 2019; Eaton et al., 2020).

106 Here, we performed a proteomic screen for new termination factors by searching for
107 proteins that bind to Pol II complexes in a manner that depends on PAS recognition by
108 CPSF30. This uncovered ZC3H4, a metazoan zinc finger-containing factor without a
109 characterised function in transcription. Because of the nature of our screen, we anticipated
110 a role for ZC3H4 in 3' end formation; however, its effects on this process are mild and apply
111 to a small number of genes. Its main function is to restrict non-coding transcription,
112 especially of PROMPT and eRNA transcripts, which are extended by hundreds of kb when
113 ZC3H4 is depleted. ZC3H4 interacts with WDR82, the depletion of which causes similar
114 defects. Tethered function assays show that ZC3H4 recruitment is sufficient to restrict
115 transcription and cause RNA degradation by the exosome. In sum, we reveal ZC3H4 as a
116 hitherto unknown terminator of promoter-proximal transcription with particular relevance at
117 non-coding loci.

118

119 **RESULTS**

120 **The effect of CPSF30 depletion on the Pol II-proximal proteome**

121 The first step of PAS recognition involves the binding of CPSF30 to the AAUAAA
122 signal (Chan et al., 2014; Clerici et al., 2018; Sun et al., 2018). We reasoned that
123 elimination of CPSF30 would impede PAS-dependent remodelling of elongation complexes
124 and cause the retention or exclusion of potentially undiscovered transcriptional termination

125 factors. We used CRISPR/Cas9 genome editing to tag *CPSF30* with a mini auxin-inducible
126 degron (mAID) (Figure 1A). The integration was performed in HCT116 cells where we had
127 previously introduced the plant F-box gene, *TIR1*, required for the AID system to work
128 (Eaton et al., 2018; Natsume et al., 2016). CPSF30-mAID is eliminated by 3 hours of indol-
129 3-acetic acid (auxin/IAA) treatment (Figure 1B). This results in profound and general
130 transcriptional read-through downstream of protein-coding genes (Figure 1C and Figure 1-
131 figure supplement 1A) demonstrating widespread impairment of PAS function.

132 To identify Pol II interactions sensitive to CPSF30, we further modified *CPSF30-*
133 *mAID* cells to homozygously tag the largest subunit of Pol II, Rpb1, with mini(m)-Turbo
134 (Figure 1D and Figure 1- figure supplement 1B). mTurbo is an engineered ligase that
135 biotinylates proximal proteins when cells are exposed to biotin (Branon et al., 2018). This
136 occurs within minutes of biotin addition to culture media, which is advantageous for
137 analysing dynamic proteins such as Pol II. We chose this approach rather than
138 immunoprecipitation (IP) because it allows isolation of weak/transient interactions (potentially
139 disrupted during conventional IP) and may identify relevant proximal proteins that do not
140 interact with Pol II directly. Importantly, CPSF30-mAID depletion still induced strong read-
141 through in this cell line (Figure 1 - figure supplement 1C).

142 *CPSF30-mAID:RPB1-mTurbo* cells were exposed to biotin before western blotting
143 with streptavidin horseradish peroxidase (HRP). This revealed multiple bands with a
144 prominent one corresponding in size to Rpb1-mTurbo and indicating the biotinylation of its
145 proximal proteome (Figure 1E). A small number of endogenously biotinylated factors were
146 observed in the absence of biotin. Biotin-exposed samples were subject to tandem mass
147 tagging (TMT) with mass spectrometry. We focused on proteins with reduced abundance
148 after auxin treatment (Supplementary File 1). The factor most depleted was CPSF30,
149 confirming that its auxin-dependent depletion is reflected in the data (Figure 1F). As
150 expected, Rpb1 was the most abundant factor in all samples consistent with its self-
151 biotinylation seen by western blotting. After CPSF30, the most depleted factors were Fip1,
152 CPSF100 and WDR33, which are in the CPSF complex. Otherwise, surprisingly few
153 proteins showed reduced signal following auxin treatment. This implies that the major effect
154 of CPSF30 depletion on the Pol II-proximal interactome is to prevent the
155 recruitment/assembly of the CPSF complex.

156

157 **ZC3H4 is a candidate transcription termination factor that is metazoan-enriched**

158 Two poorly characterised factors, ZC3H4 and ZC3H6, were the next most depleted.
159 They contain CCCH zinc finger motifs flanked by intrinsically disordered regions (Figure 1 –

160 figure supplement 2A). Their potential relationship to canonical 3' end formation factors is
161 suggested via known/predicted protein-protein interactions that are collated by the STRING
162 database (Jensen et al., 2009) (Figure 1 – figure supplement 2B). ZC3H4 is also co-
163 regulated with mRNA processing factors suggesting a role in RNA biogenesis (Figure 1 –
164 figure supplement 2C; (Kustatscher et al., 2019)). Although little is reported on ZC3H4, two
165 independent studies uncovered it as an interaction partner of WDR82 using Mass
166 Spectrometry (Lee et al., 2010; van Nuland et al., 2013). WDR82 plays a key role in
167 transcriptional termination in yeast, trypanosomes and mice (Austena et al., 2015; Kieft et
168 al., 2020; Nedea et al., 2003). To verify this interaction, we tagged ZC3H4 with GFP and
169 performed a “GFP trap” whereby ZC3H4-GFP is captured from whole cell lysates using GFP
170 nanobody-coupled beads (Figure 1 – figure supplement 2D). WDR82 robustly co-
171 coprecipitated with ZC3H4-GFP confirming them as interacting partners. Although WDR82 is
172 conserved between human and budding yeast our phylogenetic analysis suggested that
173 ZC3H4 and ZC3H6 are largely restricted to metazoans and are paralogues (Figure 1 - figure
174 supplement 3A and B).

175

176 **ZC3H4 restricts non-coding transcription events**

177 To assess any function of ZC3H4 and/or ZC3H6 in RNA biogenesis we depleted
178 either or both from HCT116 cells using RNA interference (RNAi) (Figure 2 figure supplement
179 1A), then deep sequenced nuclear transcripts. Comparison of these datasets shows that
180 ZC3H4 loss has a more noticeable impact than ZC3H6 depletion (Figure 2 – figure
181 supplement 1B). Specifically, ZC3H6 depleted samples are more similar to control than
182 those deriving from ZC3H4 loss and ZC3H4/ZC3H6 co-depletion resembles a knock-down of
183 just ZC3H4. This was also evident from closer inspection of the data (Figure 2 – figure
184 supplement 1C), supporting the phylogenetic prediction of their separate functions.
185 Accordingly, subsequent analyses focus on ZC3H4.

186 Due to its links with CPSF30 and WDR82, we anticipated that ZC3H4 might affect
187 transcriptional termination. We first checked protein-coding genes and found a small
188 number with longer read-through beyond the PAS when ZC3H4 is depleted (Figure 2A).
189 However, broader analysis suggests that this is not widespread and far fewer genes exhibit
190 increased read-through following ZC3H4 loss compared to when CPSF30 is absent (Figure
191 2B and Figure 2 – figure supplement 2A-D). Interestingly, the metagene in Figure 2B
192 revealed slightly more signal antisense of promoters when ZC3H4 is depleted. This
193 indicates an effect on non-coding RNA, which is interesting in light of a previously described
194 function for WDR82 in restricting intragenic transcription (Austena et al., 2015). These

195 PROMPT transcripts are normally rapidly degraded 3'→5' by the exosome (Preker et al.,
196 2008). Figure 2C shows an example PROMPT, upstream of *MYC*, which is undetectable in
197 control siRNA treated cells, but abundant following ZC3H4 depletion. Loss of ZC3H4 also
198 leads to the extension of this transcript by more than 100 kilobases. This is made clearer by
199 comparing the loss of ZC3H4 to AID-mediated depletion of the catalytic exosome (DIS3)
200 (Davidson et al., 2019). DIS3 depletion stabilises the usual extent of PROMPT RNA, which
201 is much shorter than when ZC3H4 is absent. Importantly, meta-analysis reveals similar
202 effects at many other PROMPTs (Figure 2D). These data strongly suggest that PROMPT
203 transcripts are stabilised and extended in the absence of ZC3H4, presumably because its
204 normal function restricts their transcription.

205 The finding that PROMPTs are affected by ZC3H4 suggested a role in the
206 transcription/metabolism of antisense/non-coding RNAs. We therefore extended our search
207 for potential ZC3H4 regulated transcription to enhancer regions since they also produce
208 short RNAs that are degraded by the exosome (Andersson et al., 2014). eRNAs can be
209 found in isolation and in clusters called super-enhancers (SEs) (Pott and Lieb, 2015). SEs
210 are thought to be important for controlling key developmental genes with strong relevance to
211 disease (Hnisz et al., 2013). ZC3H4 depletion has a clear effect over SE regions
212 exemplified by the *MYC* SE where upregulation and extension of eRNAs is obvious (Figure
213 2E). Acute depletion of DIS3 illustrates the normally restricted range of individual eRNAs
214 within the cluster. This effect is general for other SEs as demonstrated by the metaplots in
215 Figure 2F. We also checked the effect of CPSF30 depletion on example PROMPT and SE
216 transcription, which are very modest and consistent with the lack of antisense effect seen by
217 metagene in Figure 1C (Figure 2 – figure supplement 2E). Consistently, PROMPTs
218 susceptible to ZC3H4 were not enriched in PASs compared to those unaffected by it and
219 harbour a slightly lower density (Figure 2 – figure supplement 2F). Overall, these data
220 strongly suggest that ZC3H4 is important for regulating transcription across many PROMPTs
221 and SEs.

222 **Comparison of ZC3H4 and Integrator effects**

223 ZC3H4 has some functions in common with the Integrator complex. This is a
224 metazoan-specific assembly with regulatory functions at non-coding loci (Lai et al., 2015;
225 Mendoza-Figueroa et al., 2020; Nojima et al., 2018). We previously sequenced chromatin-
226 associated RNA derived from HCT116 cells RNAi depleted of the Integrator backbone
227 component INTS1 (Davidson et al., 2020). Chromatin-associated RNA is purified via
228 urea/detergent extraction and is enriched in nascent RNAs (Wuarin and Schibler, 1994).
229 Metagene analysis of this data at protein-coding genes shows a mild effect of Integrator

230 depletion over PROMPT regions (Figure 3A). It also reveals an accumulation of promoter-
231 proximal RNAs in the coding direction consistent with a recent report on its function as an
232 attenuator of protein-coding transcription (Lykke-Andersen et al., 2020). Because of this
233 function, Integrator depletion can lead to increased expression of a subset of mRNAs (Elrod
234 et al., 2019; Lykke-Andersen et al., 2020; Tatomer et al., 2019). *HAP1* is an example of a
235 gene where this is seen (Figure 3B). Similarly, we saw evidence for increased mRNA
236 expression on some genes when ZC3H4 was depleted (Figure 3C). Interestingly these two
237 genes are selectively effected by Integrator or ZC3H4 respectively and additional examples
238 of this are shown in Figure 3 – figure supplement 1A. Bioinformatic analysis revealed
239 around 1000 genes affected by INTS1 or ZC3H4 depletion with little overlap between the
240 two conditions (Figure 3D, Supplementary File 4). Indeed, analysis of recently published
241 metabolically labelled RNA-seq data from HeLa cells depleted of the catalytic Integrator
242 subunit or ZC3H4 reveals several hundred upregulated mRNAs - also with minimal overlap
243 (Austenaa et al., 2021; Lykke-Andersen et al., 2020) (Figure 3 – figure supplement 1B).
244 When searching for characteristics of these targets in our HCT116 data, we found that
245 transcripts upregulated following either ZC3H4 or INTS1 loss are normally expressed at
246 lower levels than unaffected genes (Figure 3E). This is consistent with the idea that they are
247 subject to repression by these two factors under these experimental conditions.

248 The most prominent effects of ZC3H4 were observed at PROMPT and SE regions
249 where, again, Integrator is implicated (Lai et al., 2015; Nojima et al., 2018). Where ZC3H4
250 effects are evident over PROMPT regions, they are generally more substantial than those
251 seen after Integrator loss, exemplified by the *ITPRID2* PROMPT in Figure 3F and via meta-
252 analyses (Figure 3 – figure supplement 1C and D). At SEs, ZC3H4 depletion generally
253 results in a greater stabilisation and elongation of eRNA, compared to INTS1 knock-down,
254 exemplified at the *MSRB3* SE (Figure 3G). Meta-analysis confirms less effect of INTS1
255 depletion at SEs versus the impact of ZC3H4 (compare Figures 3H and 2F). We note that
256 these INTS1 data are on chromatin-associated RNA whereas ZC3H4 images are obtained
257 from nuclear RNA. However, as chromatin-associated RNA is more enriched in nascent
258 transcripts this would be expected to capture more extended non-coding transcription and
259 not less as is the case here. Moreover, previously published analyses of Integrator effects
260 on transcription do not report the long extended non-coding (PROMPT/eRNA) transcripts
261 that we observe when ZC3H4 is depleted (Beckedorff et al., 2020; Lykke-Andersen et al.,
262 2020).

263

264 **Rapid ZC3H4 depletion and re-expression confirms the functions found by RNA-seq**

265 ZC3H4 RNAi suggests its widespread involvement in non-coding RNA synthesis and
266 the regulation of a subset of protein-coding transcripts. However, RNAi depletion was
267 performed using a 72 hr protocol and might result in indirect or compensatory effects. To
268 assess whether these effects are a more direct consequence of ZC3H4 loss, we engineered
269 HCT116 cells for its rapid and inducible depletion. CRISPR/Cas9 was used to tag *ZC3H4*
270 with an *E.coli* derived DHFR degron preceded by 3xHA epitopes (Figure 4A; (Sheridan and
271 Bentley, 2016)). In this system, cells are maintained in trimethoprim (TMP) to stabilise the
272 degron, removal of which causes protein depletion. Western blotting demonstrates
273 homozygous tagging of *ZC3H4* and that ZC3H4-DHFR is depleted following TMP removal
274 (Figure 4B). Depletion was complete after overnight growth without TMP but substantial
275 protein loss was already observed after 4 hrs allowing us to assess the consequences of
276 more rapid ZC3H4 depletion.

277 TMP-mediated depletion can also be reversed by its re-administration facilitating a
278 test of whether ZC3H4 effects are reversed by its reappearance. The western blot in Figure
279 4C illustrates this by showing that TMP withdrawal depletes ZC3H4-DHFR, which re-
280 appears following 4 hrs TMP addition. To ask whether ZC3H4 effects are an immediate
281 consequence of its loss and if they are reversed following its re-appearance, RNA was
282 isolated from the three conditions shown in the western blot. This was analysed by qRT-
283 PCR to assess the levels of extended PROMPT (*HMG2*, *ITPRID2*) and SE (*MSRB3*,
284 *DLGAP1*) RNAs (Figure 4D). All were increased following ZC3H4 loss suggesting that the
285 effects that we observed by RNAi are not due to compensatory pathways. Although 4 hr
286 TMP re-administration does not restore ZC3H4 to full levels, it was sufficient to reverse the
287 effects of its depletion at all tested amplicons. The timescale over which the effect can be
288 reversed suggests that transcripts induced by ZC3H4 loss remain relatively unstable. Rapid
289 ZC3H4 depletion also confirmed the prediction, from our RNA-seq, that the extended
290 PROMPT transcripts result from the aberrant transcription of these loci (Figure 4 – figure
291 supplement 1A and B).

292 Another key observation from our nuclear RNA-seq was the potential for ZC3H4 to
293 restrict the levels of a subset of protein-coding transcripts. The long-term nature of RNAi
294 and its detection via nuclear RNA-seq means that it could be an indirect or post-
295 transcriptional effect, respectively. To test whether mRNA upregulation is an immediate and
296 transcriptional response to ZC3H4 loss, we isolated chromatin-associated RNA from *ZC3H4*-
297 *DHFR* cells grown with or without TMP for 4 hrs. To additionally confirm their specificity to
298 ZC3H4 (vs Integrator), we also depleted the catalytic Integrator subunit utilising our
299 previously engineered cell line in which INTS11 is tagged with a small molecule assisted
300 shut-off module (Chung et al., 2015; Davidson et al., 2020). qRT-PCR was used to detect

301 three transcripts (NWD1, ENO3 and PJKV) that were upregulated by ZC3H4 loss but not
302 Integrator depletion. Spliced versions of all three were increased after 4 hrs of ZC3H4
303 depletion, but unaffected by loss of the catalytic Integrator subunit INTS11 (Figure 4E). The
304 effectiveness of INTS11 depletion is illustrated by the substantial increase in U1 snRNA
305 read-through RNA in its absence. This demonstrates that some mRNAs are immediately
306 and selectively upregulated following ZC3H4 loss.

307 We next asked whether the ZC3H4 interactor, WDR82, impacts the levels of
308 PROMPT and SE transcripts. Accordingly, *ZC3H4-DHFR* cells were treated with control or
309 WDR82-specific siRNAs (Figure 4F). We also co-depleted ZC3H4 and WDR82 by removing
310 TMP from cells first transfected with WDR82 siRNAs. WDR82 depletion enhanced the level
311 of all tested transcripts suggesting that it functionally overlaps with ZC3H4 (Figure 4G).
312 There was no synergistic effect of their co-depletion implying that WDR82 and ZC3H4 do not
313 act redundantly at the tested loci. WDR82 is found in complexes containing protein
314 phosphatase 1 (PP1) and the SETD1A/B methyl transferases (Lee et al., 2010; van Nuland
315 et al., 2013). We found that the former but not the latter is implicated in the stability of the
316 non-coding transcripts selected for this experiment (Figure 4 – figure supplement 1C-E).

317 **ZC3H4 occupies a broad region at a subset of promoters**

318 We have demonstrated that depletion of ZC3H4 causes widespread defects in non-
319 coding transcription and suppresses a subset of protein-coding RNAs. As these effects are
320 seen following rapid ZC3H4 depletion, we hypothesised that they may be directly mediated
321 by its recruitment to relevant loci. Consistently, its capture in our mTurbo experiment
322 supports its proximity to chromatin and the presence of CCCH zinc finger domains predict
323 nucleic acid binding capability. Therefore, its genomic occupancy was globally investigated
324 by performing ZC3H4 chromatin immunoprecipitation and sequencing (ChIP-seq) alongside
325 that of Pol II.

326 ZC3H4 occupies genes with binding broadly resembling that of Pol II and showing
327 the greatest enrichment over promoter regions (Figure 5A). However, many genes that are
328 occupied by Pol II do not recruit ZC3H4 (Figure 5B). This might result from low affinity of the
329 ZC3H4 antibody or that its recruitment to chromatin is bridged since ZC3H4 also directly
330 crosslinks to RNA in cells (Figure 5 – figure supplement 1A). However, its differential gene
331 occupancy is consistent with the selective effects of its depletion. Interestingly, ZC3H4
332 occupies a broader promoter region than Pol II suggesting that its function is not restricted to
333 the precise transcriptional start site. The width of this peak often corresponds to the normal
334 extent of PROMPT and eRNA transcription, which is elongated in its absence. *RPL13* is
335 shown as an example of recruitment of ZC3H4 upstream of the promoter, where its loss

336 causes stabilisation and extension of the antisense transcript (Figure 5C). ZC3H4 is also
337 strongly recruited to SEs consistent with the RNA effects observed on them following its loss
338 (Figure 5D). This is exemplified by the *MSRB3* region and generalised by metaplots in
339 figure 5E. Although our analyses of eRNA and PROMPTs were guided by our RNA-seq
340 findings, an unbiased search for peaks of ZC3H4 and Pol II signal confirmed proportionally
341 greater ZC3H4 occupancy at distal intergenic regions (encompassing SEs) (Figure 5F).

342 Overall, the HCT116 ChIP-seq demonstrates direct recruitment of ZC3H4 to potential
343 targets. One mentioned caveat is the low ChIP efficiency of the ZC3H4 antibody; however,
344 a ZC3H4 ChIP-seq experiment was recently made available by the ENCODE consortium
345 (Partridge et al., 2020). This used a flag-tagged construct and was performed in HEPG2
346 cells allowing a comparison of our data to that obtained with a high-affinity antibody and in
347 different cells. Consistent with our findings, flag-ZC3H4 occupies a subset of Pol II-bound
348 regions and shows broader distribution than Pol II around promoters (Figure 5G). Although
349 HEPG2 cells express fewer SEs than HCT116 cells, the transcribed *DLGAP1* example
350 confirms its occupancy of these regions in both cell types (Figure 5 – figure supplement 1B).
351 In contrast, the *MYC* SE is only expressed in HCT116 cells and is not occupied by ZC3H4 in
352 HEPG2 cells. In further agreement with our data, bioinformatics assignment of flag-ZC3H4
353 binding sites yielded “promoter and enhancer-like” as the most enriched terms (Partridge et
354 al., 2020).

355

356 **Engineered recruitment of ZC3H4 suppresses transcription**

357 The consequences of ZC3H4 recruitment to targets are predicted to be their early
358 termination and subsequent degradation by the exosome, based on the known fate of
359 PROMPTs and eRNAs. To test whether ZC3H4 recruitment can promote these effects, we
360 established a tethered function assay. ZC3H4 was tagged with bacteriophage MS2 coat
361 protein to engineer its recruitment to a reporter containing MS2 hairpin binding sites (MS2hp-
362 IRES-GFP; Figure 6A). Importantly, RNA from this reporter is unaffected by endogenous
363 ZC3H4 (Figure 6 – figure supplement 1A). HCT116 cells were transfected with either of
364 these three constructs together with MS2hp-IRES-GFP and reporter expression assayed by
365 qRT-PCR. Compared to the two controls, tethered ZC3H4-MS2 significantly reduced
366 reporter RNA expression (Figure 6B). ZC3H4-MS2 expression does not affect the same
367 reporter lacking MS2 hairpins (Figure 6 – figure supplement 1B). This directly demonstrates
368 that ZC3H4 recruitment is sufficient to negatively regulate RNA expression, mirroring the
369 upregulation of its endogenous targets seen when it is depleted.

370 PROMPTs and eRNAs are degraded on chromatin and we wanted to test whether
371 ZC3H4-MS2 exerted its effect on these nascent RNAs. The reporter experiments above are
372 on total RNA so whether ZC3H4-MS2 exerted its effect at the gene (plasmid) or following its
373 release was uncertain. Therefore, we purified chromatin-associated RNA using a salt and
374 urea-based extraction (Wuarin and Schibler, 1994). As mentioned previously, this
375 fractionation enriches nascent endogenous RNAs. However, nascent RNAs associated with
376 transfected plasmids also co-purify within this fraction (Dye et al., 2006). Accordingly, cells
377 were transfected with MS2hp-IRES-GFP and either ZC3H4-MS2 or MS2-GFP. We included
378 an additional primer set to detect RNA uncleaved at the bovine growth hormone (BGH)
379 poly(A) site. Because poly(A) site cleavage is co-transcriptional, this primer set should
380 robustly detect Pol II-associated transcripts. This amplicon and that upstream of the MS2
381 hairpins were reduced in this chromatin fraction, strongly suggesting that tethered ZC3H4
382 acts on nascent RNA (Figure 6C).

383 The exosome targets released PROMPT and eRNA transcripts, which could be
384 promoted by ZC3H4. The results we present for endogenous loci are consistent with this
385 since PROMPTs and eRNAs are upregulated and elongated when ZC3H4 is depleted. To
386 test whether recruited ZC3H4 leads to exosome decay, we transfected MS2hp-IRES-GFP,
387 together with either MS2-GFP or ZC3H4-MS2, into *DIS3-AID* cells that were then treated or
388 not with auxin to eliminate the catalytic exosome. RNA upstream and downstream of the
389 MS2 hairpins was detected by qRT-PCR and their ratio plotted (Figure 6D). Enhanced
390 levels of upstream versus downstream amplicon were associated with transfection of
391 ZC3H4-MS2 and is more prominent after depletion of DIS3. This is consistent with the
392 hypothesis that recruited ZC3H4 promotes the release of RNA that is a DIS3 substrate
393 (Figure 6E). Results presented above show that ZC3H4 functions in transcriptional
394 regulation. ZC3H4 may also regulate the stability of its targets; however, to our knowledge,
395 it has not been found to prominently co-purify with the exosome.

396 Finally, we were interested to determine the overall relevance of ZC3H4 to cell
397 health/growth. This is made simpler by the *ZC3H4-DHFR* cell line, which allows permanent
398 depletion of ZC3H4 by culturing cells without TMP. Accordingly, we performed colony
399 formation assays on these cells grown in the presence or absence of TMP (Figure 6F). Loss
400 of ZC3H4 was associated with smaller colonies, which demonstrates the importance of
401 ZC3H4 for growth/proliferation.

402

403 **DISCUSSION**

404 We have discovered that ZC3H4 controls unproductive transcription, especially at
405 non-coding loci. This conclusion is based on its recruitment to loci that give rise to
406 transcripts that are stabilised and elongated when it is depleted. Moreover, tethering ZC3H4
407 to a heterologous reporter RNA is sufficient to promote degradation of the transcript by the
408 exosome. We propose that ZC3H4 recruitment drives some of the early transcriptional
409 termination that is characteristic of many non-coding RNAs, particularly PROMPT and eRNA
410 transcripts. The function of ZC3H4 in restraining their transcription may at least partly
411 explain why PROMPT and eRNA transcripts accumulate as short species when the
412 exosome is depleted.

413 Our discovery of ZC3H4 adds to an increasing number of termination pathways. Most
414 of these are more relevant during the initial stages of transcription, rather than the more
415 intensively studied process that occurs at the end of protein-coding genes. This is evident
416 from comparing the general requirement for CPSF30 at the 3' end of protein-coding genes
417 with the more selective impact of ZC3H4 that is focused more promoter-proximally. The
418 effects of ZC3H4 depletion are reminiscent of recent findings on the Integrator complex,
419 which also controls the early termination of transcription (Elrod et al., 2019; Lykke-Andersen
420 et al., 2020; Tatomer et al., 2019). Our initial comparison of transcripts sensitive to either
421 Integrator or ZC3H4 suggests that they can act on separate RNA targets. An exciting
422 possibility is that multiple early termination pathways may contribute to conditional gene
423 regulation. It will be important to establish whether ZC3H4 and/or Integrator are naturally
424 utilised to regulate transcription in this manner. Their predominance in metazoans may
425 enable complex gene regulation, for example across cell types or during development.

426 ZC3H4 has been proposed as an equivalent to *Drosophila* Suppressor of Sable
427 (Su(s)), which negatively regulates transcription via promoter-proximal termination (Brewer-
428 Jensen et al., 2016; Kuan et al., 2004). ZC3H4 and Su(s) share little sequence homology,
429 but they have similar structural makeup with zinc fingers flanked by largely disordered
430 regions. Su(s) depletion stabilises selected RNAs and causes their aberrant elongation and
431 stability, mirroring what we see globally following ZC3H4 depletion. There is no known
432 catalytic activity for ZC3H4 or Su(s), but they are related to CPSF30 which shows
433 endonuclease activity in *Drosophila* and *Arabidopsis* (Addepalli and Hunt, 2007; Bai and
434 Tolia, 1996). It remains to be seen whether ZC3H4 possesses any catalytic activity or
435 mediates its effects through interaction partners. Interestingly, IP and mass spectrometry
436 indicates that WDR82 may be the only interacting partner of Su(s) (Brewer-Jensen et al.,
437 2016). WDR82 has been shown to bind to Pol II phosphorylated on Serine 5 of its C-
438 terminal domain, which may provide a means to recruit ZC3H4 to promoter-proximal regions
439 (Lee and Skalnik, 2008).

440 The recruitment of ZC3H4 to promoters is consistent with our observation that
441 promoter-proximal transcription is most affected by its absence. Since depletion of ZC3H4
442 causes extended transcription of its targets, it is reasonable to suppose that it normally
443 restricts their transcription in some fashion. This might be by controlling the escape of
444 promoter-proximally paused polymerases or by acting closer to the 3' end of its target
445 transcripts. The fact that ZC3H4 acts somewhat selectively (e.g. not all PROMPTs and
446 mRNAs are its targets) suggests that elements of specificity are required to explain its
447 mechanism. Most obviously, this could be sequences within DNA or RNA, to which ZC3H4
448 (and Su(s)) binds via CHIP and XRNAX, respectively (see Figure 5 and Figure 5 – figure
449 supplement 1A). While our paper was under revision, another report identified ZC3H4 as
450 affecting the transcription of intragenic loci in mammalian cells (Austenaa et al., 2021). In
451 agreement with our findings, non-coding transcripts were affected by ZC3H4 depletion. It
452 was proposed to terminate some non-coding transcripts as a result of spurious/weak
453 splicing. Similarly, Su(s) regulation of transcription was linked to the presence of a cryptic 5'
454 splice site (Kuan et al., 2004). This suggests involvement with U1 snRNA, which recognises
455 this sequence. While U1 snRNA inhibition does cause some stabilisation of PROMPTs, it
456 does not generally result in their longer extension and so other *cis*-acting sequences and
457 processes may additionally contribute (Oh et al., 2017). Our evidence that ZC3H4 binds
458 RNA in cells suggests that it may directly interact with some of its target transcripts and it will
459 be important to delineate any sequence determinants.

460 Beyond transcriptional regulation, ZC3H4 occupancy of SEs is interesting. Other
461 notable SE-associated factors (e.g. BRD4 and MED1) are much more generally implicated in
462 Pol II transcription than ZC3H4 (Sabari et al., 2018). Moreover, they are transcriptional
463 activators whereas ZC3H4 appears to suppress transcription (or, at least, its RNA output).
464 Many SE-bound factors are found to have phase separation properties explaining why large
465 clusters of factors accumulate at these regions (Cho et al., 2018). While we do not know
466 whether ZC3H4 can phase separate, it contains large regions of intrinsic disorder, which can
467 promote this property (Figure 1 – figure supplement 2A). In general, ZC3H4 may offer a new
468 way to study enhancer clusters, particularly the importance of restricting transcription across
469 these regions.

470 In conclusion, we have uncovered ZC3H4 as a factor with a function in restricting
471 transcription. Its most notable effects are at non-coding loci where transcriptional
472 termination mechanisms are less understood than at protein-coding genes. Further
473 dissection of ZC3H4 and its targeting should reveal additional important insights into how
474 this unstable portion of the transcriptome is controlled. The non-overlapping effects of

475 Integrator and ZC3H4 at protein-coding genes indicate the possibility that multiple factors
476 may control gene output via premature transcriptional termination.

477

478 **ACKNOWLEDGEMENTS**

479 We are grateful to the other members of the lab for critical comment. This work was
480 supported by a Wellcome Trust Investigator Award (WT107791/Z/15/Z) and a Lister Institute
481 Research Fellowship held by S.W. We are grateful to The University of Exeter Sequencing
482 Service where all sequencing was performed who are supported by a Medical Research
483 Council Clinical Infrastructure Award (MR/ M008924/1), the Wellcome Trust Institutional
484 Strategic Support Fund (WT097835MF), a Wellcome Trust Multi User Equipment Award
485 (WT101650MA), and a Biotechnology and Biological Sciences Research Council Longer and
486 Larger (LoLa) Award (BB/ K003240/1).

487

488 **MATERIALS AND METHODS**

Key Resources Table				
Reagent type (species) or resource	Designation	Source or reference	Identifiers	Additional information
Cell line (Human)	HCT116-CPSF30-mAID	In-house	This paper	
Cell line (Human)	HCT116-CPSF30-mAID:RPB1-mTurbo	In-house	This paper	
Cell line (Human)	HCT116-ZC3H4-HA-DHFR	In-house	This paper	
Cell line (Human)	HCT116-DIS3-AID	In-house	PMID: 30840897	

Cell line (Human)	HCT116- PNUTS-AID	In-house	This paper	
Cell line (Human)	HCT116- INTS11- SMASh	In-house	PMID: 33113359	
Recombinant DNA reagent	3xHA- mTurbo- NLS_pCDNA 3	Addgene	RRID #: Addgene_107172	
Recombinant DNA reagent	px300	Addgene	RRID #: Addgene_42230	
Recombinant DNA reagent	ZC3H4- pcDNA3.1(+)- C-eGFP	Genscript	Custom synthesis	ENTS000002 53048
Recombinant DNA reagent	pSL-MS2-6x	Addgene	RRID #: Addgene_27118	
Recombinant DNA reagent	pcDNA3.1(+) IR ES GFP	Addgene	RRID #: Addgene_51406	
Antibody	CPSF30	Bethyl	RRID #: AB_2780000 Cat #: A301-585A-T	(1:1000)
Antibody	RNA Pol II	Abcam	RRID #: AB_306327 Cat #: ab817	Now discontinued at abcam (1:1000 for western blot. 4-5ug used for ChIP qPCR and -seq, respectively)

Antibody	PNUTS	Bethyl	RRID #: AB_2779219 Cat #: A300-439A-T	(1:1000)
Antibody	WDR82	Cell Signalling	RRID #: AB_2800319 Clone: D2I3B Cat #: 99715	(1:1000)
Antibody	EXOSC10	Santa Cruz	RRID #: AB_10990273 Cat #: sc-374595	(1:2000)
Antibody	ZC3H4	Atlas Antibodies	RRID #: AB_10795495 Cat #: HPA040934	(1:1000)
Antibody	HA tag	Roche	RRID #: AB_390918 Clone: 3f10 Cat #: 11867423001	(1:2000)
Antibody	GFP	Chromotek	Clone: PABG1 Cat #: PABG1-100 RRID #: AB_2749857	(1:2000)
Antibody	TCF4/TCF7L2	Cell Signalling	RRID #: AB_2199816 Clone: C48H11 Cat #: 2569	(1:1000)
Chemical compound drug	TMP	Sigma	Cat #: T7883	
Chemical compound drug	IAA	Sigma	Cat #: 12886	
Commercial assay, kit	Lipofectamine RNAiMax	Life Technologies	Cat #: 13778075	

Commercial assay, kit	JetPRIME	PolyPlus	Cat #: 114-01	
Commercial assay, kit	Streptavidin Sepharose High Performance slurry	GE Healthcare	Cat #: GE28-9857-38	
Commercial assay, kit	GFP TRAP magnetic agarose	Chromotek	RRID #: AB_2827592 Cat #: gtd-100	
Commercial assay, kit	Dynabeads α -Mouse	Life Technologies	RRID #: AB_2783640 Cat #: 11201D	
Commercial assay, kit	Dynabeads α -Rabbit	Life Technologies	RRID #: AB_2783009 Cat #: 11203D	
Commercial assay, kit	SimpleChIP® Plus Enzymatic Chromatin kit	Cell Signalling	Cat #: 9005	
Commercial assay, kit	TruSeq Stranded Total RNA Library Prep Kit	Illumina	Cat #: 20020596	
Commercial assay, kit	NEBNext® Ultra™ II DNA Library Prep Kit for Illumina®	NEB	Cat #: E7645S	
Commercial assay, kit	Ribo-Zero Gold rRNA removal kit	Illumina	Cat #: 20040526	

Commercial assay, kit	Ampure XP beads	Beckman Coulter	Cat #: A63880	
Commercial assay, kit	RNAClean XP Beads	Beckman Coulter	Cat #: A63987	
Software, algorithm	BamTools	(Barnett et al., 2011)	RRID #: SCR_015987	v2.4.0
Software, algorithm	BEDtools	(Quinlan and Hall, 2010)	RRID #: SCR_006646	v2.26.1
Software, algorithm	Bioconductor	https://bioconductor.org/	RRID #: SCR_006442	v3.11
Software, algorithm	DeepTools	(Ramirez et al., 2014)	RRID #: SCR_016366	v3.3.0
Software, algorithm	DESeq2	(Love et al., 2014)	RRID #: SCR_015687	v1.28.1
Software, algorithm	featureCounts	(Liao et al., 2013, 2014)	RRID #: SCR_012919	v2.0.0
Software, algorithm	FIMO	(Grant et al., 2011)	RRID #: SCR_001783	v5.3.3
Software, algorithm	genomicRanges	http://bioconductor.org/packages/release/bioc/html/GenomicRanges	RRID #: SCR_000025	v1.40.0
Software, algorithm	ggplot2	https://cran.r-project.org/web/packages/ggplot2	RRID #: SCR_014601	v3.3.3

Software, algorithm	Hisat2	(Kim et al., 2015)	RRID #: SCR_015530	v2.1.0
Software, algorithm	IGV	(Robinson et al., 2011)	RRID #: SCR_011793	v2.8.2
Software, algorithm	MACS2	(Zhang et al., 2008)	RRID #: SCR_013291	v2.2.6
Software, algorithm	pheatmap	https://cran.r-project.org/web/packages/pheatmap	RRID #: SCR_016418	v1.0.12
Software, algorithm	R	https://cran.r-project.org/	NA	v4.0.4
Software, algorithm	Rstudio	https://rstudio.com/	RRID #: SCR_000432	v1.3.1093
Software, algorithm	rtracklayer	https://bioconductor.org/packages/release/bioc/html/rtracklayer	NA	v1.48.0
Software, algorithm	SAMTools	(Li et al., 2009)	RRID #: SCR_002105	v.1.11
Software, algorithm	Trim_galore!	https://github.com/FelixKrueger/TrimGalore/	RRID #: SCR_011847	v.0.6.5dev

489

490 **Cell culture**

491 HCT116 parental cells and engineered cell lines were tested negative for
492 mycoplasma and cultured in Dulbecco modified eagle medium, supplemented with 10%
493 foetal calf serum and penicillin streptomycin (Gibco). For RNAi, 6 or 24-well dishes were
494 transfected with siRNA using Lipofectamine RNAiMax (Life Technologies) following the
495 manufacturers' guidelines. The transfection was repeated 24 hours later and, 48 hours after

496 the first transfection, RNA was isolated. For MS2 assays, cells were seeded in 24-well
497 dishes overnight, then transfected with 50ng MS2hp-IRES-GFP and 100ng of MS2-GFP,
498 ZC3H4-MS2 or ZC3H4-GFP using JetPRIME® (PolyPlus) for 24 hours. To deplete DIS3-
499 AID or PNUTS-AID, auxin was used at a final concentration of 500uM. To deplete ZC3H4-
500 DHFR, cells were washed twice in PBS and grown in media with or without TMP (30uM).

501 **Cell line generation and cloning**

502 *CPSF30-mAID* and *CPSF30-mAID:RBP1-mTurbo* cells were generated using
503 CRISPR/Cas9-mediated homology-directed repair (HDR). CPSF30 and RBP1 homology
504 arms and gRNA sequences are detailed in Supplementary File 7. The mTurbo insert derives
505 from 3xHA-mTurbo-NLS_pCDNA3 (#107172, Addgene). For ZC3H4 degron cells, 3xHA-
506 DHFR was amplified from existing CPSF73-HA-DHFR constructs (published in (Eaton et al.,
507 2018)) using non-homologous end-joining (NHEJ) as described in (Manna et al., 2019).
508 PNUTS-AID cells were constructed using the protocol described in (Davidson et al., 2019).
509 In general, 6cm dishes of cells were transfected with 1ug of guide RNA expressing px300
510 plasmid (#42230, Addgene) and 1ug of each HDR template/NHEJ PCR product. Three days
511 later cells were seeded, as appropriate, into hygromycin (30µg/ml, final) neomycin
512 (800µg/ml, final) or puromycin (1µg/ml, final). ZC3H4 cDNA was purchased from Genscript
513 in a pcDNA3.1(+)-C-eGFP vector. The MS2hp-IRES-GFP reporter was made by inserting a
514 BamH1/EcoRV restriction fragment from pSL-MS2-6x (#27118, Addgene) into
515 pcDNA3.1(+)-IRES GFP (#51406, Addgene) also digested with BamH1/EcoRV.

516 **Turbo sample preparation**

517 10 cm dishes at ~80% confluency were labelled with 500 µM biotin for 10 mins and
518 the labelling reaction quenched immediately by washing cells in ice cold PBS. Cells were
519 lysed in RIPA buffer (150 mM NaCl, 1% NP40, 0.5% sodium deoxycholate, 0.1% SDS, 50
520 mM Tris-HCl at pH 8, 5 mM EDTA at pH 8) containing protease inhibitors (cOmplete mini
521 EDTA-free tablets, Roche) for 30 mins on ice, then clarified *via* centrifugation. 350 uL of
522 washed Streptavidin Sepharose High Performance slurry (GE Healthcare) was incubated
523 with biotinylated or control lysates with inversion at room temperature for 1 hour. Samples
524 were then washed twice with RIPA buffer, twice with Urea buffer (2 M urea, 50 mM Tris HCl
525 pH 8), twice with 100 mM sodium carbonate and once with (20 mM Tris HCl pH 8, 2 mM
526 CaCl₂). Residual final wash buffer was used to re-suspend the beads, which were then flash
527 frozen in liquid nitrogen and sent for Tandem Mass Spectrometry at The University of Bristol
528 Proteomics Facility.

529

530 **Identifying mass spectrometry candidates**

531 First, contaminant proteins (e.g. keratin) or those that are known to be preferentially
532 biotinylated in ligase assays (e.g. AHNAK) were excluded. Samples with an average
533 abundance ratio of ≤ 0.70 were classified as having a decreased interaction with RNA
534 polymerase II following CPSF30 depletion. Finally, proteins with ≤ 5 peptides were
535 discarded. Remaining candidates were plotted in Figure 1F.

536 **qRT-PCR**

537 1 μ g of total RNA (DNase treated) was reversed transcribed using random hexamers
538 according to manufacturer's instructions (Protoscript II, NEB); cDNA diluted to 50 μ L. qPCR
539 was performed using LUNA SYBR (NEB) on a Rotorgene (Qiagen). Fold changes were
540 calculated using Qiagen's software based on delta CT values. Graphs were plotted using
541 Prism (GraphPad). Numbers underpinning qPCR-derived bar graphs are provided in source
542 data file 1.

543 **Antibodies**

544 CPSF30 (A301-585A-T, Bethyl), RNA Pol II (ab817, Abcam), PNUTS (A300-439A-T,
545 Bethyl), WDR82 (D2I3B, Cell Signalling), EXOSC10 (sc-374595, Santa Cruz), ZC3H4
546 (HPA040934, Atlas Antibodies), HA tag (clone 3f10, 11867423001, Roche), GFP (PABG1,
547 Chromotek), TCF4/TCF7L2 (C48H11, Cell Signalling). Uncropped western blots are
548 provided in source data file 2.

549 **GFP Trap**

550 10 cm dishes were transfected (5 μ g plasmid, 24 hrs), washed with PBS and lysed for
551 30 mins on ice in 1 mL lysis buffer (150 mM NaCl, 2.5 mM MgCl₂, 20 mM Tris HCl pH 7.5, 1
552 % Triton X-100, 250 units Benzonase [Sigma]). Samples were then clarified through
553 centrifugation (12000xg, 10 mins), split in two and incubated with 25 μ L of GFP TRAP
554 magnetic agarose (Chromotek) for 1hr with rotation at 4°C. Beads were washed 5x with
555 lysis buffer and samples eluted by boiling in 2xSDS buffer before analysis by western
556 blotting.

557 **Nuclear RNA-Seq**

558 Nuclei were extracted from 1x 30mm dish of cells per condition using hypotonic lysis
559 buffer (10 mM Tris pH5.5, 10 mM NaCl, 2.5 mM MgCl₂, 0.5% NP40) with a 10% sucrose
560 cushion and RNA was isolated using Tri-reagent. Following DNase treatment, RNA was
561 Phenol Chloroform extracted and ethanol precipitated. After assaying quality control using a
562 Tapestation (Agilent), 1 μ g RNA was rRNA-depleted using Ribo-Zero Gold rRNA removal kit
563 (Illumina) then cleaned and purified using RNAClean XP Beads (Beckman Coulter). Libraries

564 were prepared using TruSeq Stranded Total RNA Library Prep Kit (Illumina) and purified
565 using Ampure XP beads (Beckman Coulter). A final TapeStation D100 screen was used to
566 determine cDNA fragment size and concentration before pooling and sequencing using
567 HiSeq2500 (Illumina).

568 **ChIP-qPCR**

569 Cells were cross-linked for 10 mins at room temperature (1% Formaldehyde) and
570 quenched for 5 mins (125mM Glycine). Cells were washed in PBS, pelleted (500xg) and
571 resuspended in 400ul RIPA buffer (150 mM NaCl, 1% NP40, 0.5% sodium deoxycholate,
572 0.1% SDS, 50 mM Tris-HCl at pH 8, 5 mM EDTA at pH 8). Sonication was then performed
573 in a Bioruptor (30 seconds on/30 seconds off x10 on high setting) and debris pelleted
574 (13000rpm x 10mins). Supernatants were then incubated for 2hr at 4°C with 40ul of sheep
575 anti-mouse dynabeads to which 4ug of anti-Pol II (or, as a control, nothing) was pre-bound.
576 Beads were washed 6x with RIPA buffer and then bound chromatin was eluted by 30 min
577 incubation at room temperature with rotation (500ul 0.1 M NaHCO₃ + 1% SDS). Cross-links
578 were reversed overnight at 65°C with the addition of 20ul 5M NaCl. Following phenol
579 chloroform extraction and ethanol precipitation, chromatin was resuspended in 100ul water
580 of which 1ul was used per qPCR reaction.

581 **ChIP-Seq**

582 ChIP libraries were prepared using SimpleChIP® Plus Enzymatic Chromatin kit
583 (9005, Cell Signalling) according to manufacturer's instructions. 5µg of RNA Pol II (abcam,
584 8WG16) or ZC3H4 (HPA040934, Atlas Antibodies) were used for immunoprecipitation,
585 Dynabeads α-Mouse / α-Rabbit (Life Technologies) were used for capture.

586 **Chromatin RNA isolation**

587 HCT116 cells were scraped into PBS, pelleted, incubated in hypotonic lysis buffer
588 (HLB; 10 mM Tris.HCl at pH 7.5, 10 mM NaCl, 2.5 mM MgCl₂, 0.5% NP40), underlayered
589 with 10% sucrose (w/v in HLB) on ice for 5 mins, then spun at 500 xg to isolate nuclei.
590 Supernatant and sucrose was removed and nuclei re-suspended in 100 µL of NUN1 (20 mM
591 Tris-HCl at pH 7.9, 75 mM NaCl, 0.5 mM EDTA, 50% glycerol, 0.85 mM DTT), before being
592 incubated with 1 mL NUN2 (20 mM HEPES at pH 7.6, 1 mM DTT, 7.5 mM MgCl₂, 0.2 mM
593 EDTA, 0.3 M NaCl, 1 M urea, 1% NP40) on ice for 15 mins. Samples were spun at 13, 000
594 xg to pellet chromatin, this was dissolved in Trizol and RNA extracted.

595 **Colony formation assays**

596 *ZC3H4-DHFR* cells were seeded into 100mm dishes and maintained in the presence
597 or absence of TMP for 10 days, with media replaced every 3 days. Colonies were fixed in
598 ice cold methanol for 10 mins and then stained with 0.5% crystal violet (in 25% methanol) for
599 10 minutes.

600 **XRNAX**

601 We essentially followed the protocol of (Trendel et al., 2019). HCT116 cells were
602 grown overnight in the presence or absence of doxycycline in 10 cm dishes. 24 hr later,
603 dishes were washed with PBS, UV cross linked (Stratalinker 1800 150 mJ/cm²), or not, then
604 re-suspended in 4.5 mL Trizol (Sigma). 300 uL of chloroform was added, samples agitated
605 on a ThermoMixer (Eppendorf) for 5 mins, spun at 12000xg for 15 minutes, then the
606 interphase carefully aspirated into fresh tubes. The interphase was washed thrice with Tris-
607 SDS (10 mM Tris-HCL pH 7.5, 1 mM EDTA, 0.1 % SDS), before being dissolved in 1 mL
608 Tris-SDS. 1 uL glycogen, 60 uL of 5M NaCl and 1 mL isopropanol were added and samples
609 precipitated at -20°C for 10 minutes, then pelleted at 18, 000xg for 15 mins. Precipitated
610 protein was washed with 70 % ethanol, air dried, re-suspended in 180 uL water and pellets
611 dissolved on ice. DNA was removed via TurboDNase (ThermoFisher) treatment, before
612 samples were re-pelleted, re-dissolved in RNase buffer (150 mM NaCl, 20 mM Tris-HCL pH
613 7.5, 2.5 mM MgCl₂) and RNA digested with RNase H (NEB) and 1 uL of RNase T1 (Roche).
614 4 x SDS loading buffer was added before gel electrophoresis and western blotting.

615 **Computational analysis**

616 All sequencing data were uploaded to the Galaxy web platform and processed as
617 detailed below; usegalaxy.org and usegalaxy.eu servers were used.

618 **Datasets (GEO accessions)**

619 Data newly generated in this paper (GSE163015); Pol II HEPG2 ChIP-seq
620 (GSE32883); ZC3H4 HEPG2 ChIP-seq (GSE104247); DIS3-AID HCT116 RNA-seq
621 (GSE120574); INTS1 RNAi Chromatin-associated RNA-seq (GSE150238). 4sU labelled
622 RNA differential expression in HeLa cells depleted of INTS11 or ZC3H4 (GSE133109,
623 GSE151919).

624 **RNA-Seq alignment**

625 FASTA files were trimmed using Trim Galore! and mapped to GRCh38 using HISAT2
626 using default parameters (Kim et al., 2015). Reads with a MAPQ score of ≤ 20 were
627 removed from alignment files using SAMtools (Li et al., 2009). Finally, BigWig files were
628 generated using DeepTools and visualised using IGV (Ramirez et al., 2014).

629 **ChIP alignment and visualisation**

630 All samples were mapped against GRCh38 using BWA, default settings. Reads with
631 a MAPQ score of ≤ 20 were removed along with PCR duplicates from alignment files using
632 SAMtools. Processed BAM files were converted to BigWig files using DeepTools: all
633 samples were normalised to RPKM with a bin size of 1. Aligned files were visualised using
634 IGV.

635 **ChIP peak calling**

636 For ZC3H4 and INPUT, broad peaks were called separately using MACS2 with a
637 changed “lower mfold” (2) and default settings. For each experiment, bedtools was used to
638 establish common peaks from individual reps (Intersect Intervals), creating a bed file of high
639 confidence peaks. For ZC3H4, peaks called in the INPUT sample were subtracted *via*
640 bedtools. All bed files were annotated and plotted in R using ChipSeeker (Yu et al., 2015).

641 **Gene heatmaps**

642 For ChIP heatmaps, computematrix (DeepTools) was used to generate score files
643 from ChIP bigwig files using an hg38 bed file; parameters used for each heat map are
644 detailed in figure legends. Plots were redrawn in R. Transcription read-through analysis was
645 calculated for each condition by comparing the first 1 kb downstream of the TES to a 500 bp
646 region directly preceding the TES (PAS). A log₂ ratio (depletion/control) was then applied to
647 identify increased read-through.

648 **Super-enhancer metaplots**

649 A bed file with the coordinates of super-enhancer locations from dbSUPER in
650 HCT116 cells was used as a basis (Khan and Zhang, 2016). All regions that had clusters of
651 MED1, Pol II and H3K27ac ChIP signal were retained as *bone fide* regions of interest, those
652 without were discarded. A log₂ ratio of experiment vs input was prepared using
653 BamCompare of DeepTools - for RNAseq metaplots, BAM files were split by strand. A score
654 file for the regions in the amended SE bed file was generated *via* the computematrix function
655 of DeepTools using the log₂ BamCompare output file. Results were plotted in R-studio using
656 ggplot2.

657 **Gene plots and metaplots**

658 Split strand metagene plots were generated using RPKM normalised sense and
659 antisense (scaled to -1) bigwig coverage files separately with further graphical processing
660 performed in R. For identifying ZC3H4 PROMPT regions ncRNA genes were filtered from
661 hg38 refgene gtf file to give protein-coding genes that were used with feature counts on

662 siCont RNAseq (Liao et al., 2014), to gain read count and gene length. Transcripts per
663 million (TPM) were calculated for each gene and genes with an expression of < 5 were
664 filtered out to give a list of expressed genes. Next, divergent promoters, or genes with
665 neighbours within 5kb of their promoter, were excluded to minimise background. Finally, this
666 gene list was converted to a bed file, then computematrix (DeepTools) used to generate a
667 score file from log2 siCont Vs condition bigwigs; results were plotted in R.

668 **Differential gene expression**

669 FeatureCounts was used to count mapped reads over exons and differential
670 expression was performed using DESeq2 (Liao et al., 2014; Love et al., 2014).

671 **PROMPT poly-A site detection**

672 For PROMPT analysis, we used a catalogue of 961 PROMPTs generated by *de novo*
673 assembly following acute DIS3 depletion (Davidson et al., 2019). Due to the variable length
674 of each PROMPT, we searched for the two consensus poly-A site motifs (AWTAAA) across
675 the full transcript sequence using FIMO (online). We then calculated the total occurrence of
676 poly-A sites across each PROMPT transcript per kb and separated them into two groups;
677 those that show upregulation ($\log_2FC \geq 1$) in the absence of ZC3H4 and those with no
678 change of downregulated expression. Plots were drawn in R.

679

680 **ZC3H4 homologue identification**

681 To identify ZC3H4 homolog protein sequences, sequences from UniRef100 (UniProt
682 Consortium, 2014) were searched using a profile HMM search: 'hmmsearch', part of HMMer
683 V3.2.1 (Eddy, 2011), with PANTHER (Mi et al., 2019) hidden Markov model PTHR13119,
684 corresponding to zinc finger CCCH-domain containing proteins. Profile HMM search hits
685 were filtered using a 1e-100 e-value threshold; this search identified 1513 UniRef100
686 sequences with PTHR13119 domains (representing a total of 1646 UniProtKB sequences).
687 PTHR13119 domains from human and mouse were aligned using Toffee Expresso mode
688 (Armougom et al., 2006), and multiple sequence alignment figure (Figure 1 – figure
689 supplement 3B) was rendered with ESPscript (Robert and Gouet, 2014).

690 **Phylogenetic tree reconstruction**

691 Identified PTHR13119 domains were aligned using MAFFT v7.4 (Kato and
692 Standley, 2013); sites composed of more than 75% of gaps were removed from the multiple
693 sequence alignment with trimAl (Capella-Gutierrez et al., 2009). The PTHR13119 domain
694 phylogeny was reconstructed under maximum likelihood with IQ-TREE v1.6.9 (Nguyen et al.,

695 2015). The best-fitting substitution matrix was determined by ModelFinder (Kalyaanamoorthy
696 et al., 2017), as implemented in IQ-TREE. Branch support values were based on 1000
697 ultrafast bootstraps (Minh et al., 2013). Phylogenetic Tree figure was rendered with iTOL
698 (Letunic and Bork, 2019). Multiple sequence alignment and phylogenetic tree files are
699 deposited on Zenodo (<https://doi.org/10.5281/zenodo.4637127>).

700 **Primers, siRNAs and other nucleic acid sequences**

701 Sequences are provided in Supplementary File 7.

702

703 **REFERENCES**

704 Addepalli, B., and Hunt, A.G. (2007). A novel endonuclease activity associated with the
705 Arabidopsis ortholog of the 30-kDa subunit of cleavage and polyadenylation specificity
706 factor. *Nucleic acids research* *35*, 4453-4463.

707 Andersson, R., Refsing Andersen, P., Valen, E., Core, L.J., Bornholdt, J., Boyd, M., Heick
708 Jensen, T., and Sandelin, A. (2014). Nuclear stability and transcriptional directionality
709 separate functionally distinct RNA species. *Nat Commun* *5*, 5336.

710 Armougom, F., Moretti, S., Poirot, O., Audic, S., Dumas, P., Schaeli, B., Keduas, V., and
711 Notredame, C. (2006). Expresso: automatic incorporation of structural information in multiple
712 sequence alignments using 3D-Coffee. *Nucleic acids research* *34*, W604-608.

713 Austenaa, L.M., Barozzi, I., Simonatto, M., Masella, S., Della Chiara, G., Ghisletti, S.,
714 Curina, A., de Wit, E., Bouwman, B.A., de Pretis, S., *et al.* (2015). Transcription of
715 Mammalian cis-Regulatory Elements Is Restrained by Actively Enforced Early Termination.
716 *Molecular cell* *60*, 460-474.

717 Austenaa, L.M.I., Piccolo, V., Russo, M., Prosperini, E., Polletti, S., Polizzese, D., Ghisletti,
718 S., Barozzi, I., Diaferia, G.R., and Natoli, G. (2021). A first exon termination checkpoint
719 preferentially suppresses extragenic transcription. *Nat Struct Mol Biol*.

720 Bai, C., and Tolia, P.P. (1996). Cleavage of RNA hairpins mediated by a developmentally
721 regulated CCCH zinc finger protein. *Molecular and cellular biology* *16*, 6661-6667.

722 Baillat, D., Hakimi, M.A., Naar, A.M., Shilatifard, A., Cooch, N., and Shiekhattar, R. (2005).
723 Integrator, a multiprotein mediator of small nuclear RNA processing, associates with the C-
724 terminal repeat of RNA polymerase II. *Cell* *123*, 265-276.

725 Barnett, D.W., Garrison, E.K., Quinlan, A.R., Stromberg, M.P., and Marth, G.T. (2011).
726 BamTools: a C++ API and toolkit for analyzing and managing BAM files. *Bioinformatics* *27*,
727 1691-1692.

728 Beckedorff, F., Blumenthal, E., daSilva, L.F., Aoi, Y., Cingaram, P.R., Yue, J., Zhang, A.,
729 Dokaneheifard, S., Valencia, M.G., Gaidosh, G., *et al.* (2020). The Human Integrator

730 Complex Facilitates Transcriptional Elongation by Endonucleolytic Cleavage of Nascent
731 Transcripts. *Cell reports* 32, 107917.

732 Branon, T.C., Bosch, J.A., Sanchez, A.D., Udeshi, N.D., Svinkina, T., Carr, S.A., Feldman,
733 J.L., Perrimon, N., and Ting, A.Y. (2018). Efficient proximity labeling in living cells and
734 organisms with TurboID. *Nat Biotechnol* 36, 880-887.

735 Brewer-Jensen, P., Wilson, C.B., Abernethy, J., Mollison, L., Card, S., and Searles, L.L.
736 (2016). Suppressor of sable [Su(s)] and Wdr82 down-regulate RNA from heat-shock-
737 inducible repetitive elements by a mechanism that involves transcription termination. *Rna* 22,
738 139-154.

739 Capella-Gutierrez, S., Silla-Martinez, J.M., and Gabaldon, T. (2009). trimAl: a tool for
740 automated alignment trimming in large-scale phylogenetic analyses. *Bioinformatics* 25,
741 1972-1973.

742 Chan, S.L., Huppertz, I., Yao, C., Weng, L., Moresco, J.J., Yates, J.R., 3rd, Ule, J., Manley,
743 J.L., and Shi, Y. (2014). CPSF30 and Wdr33 directly bind to AAUAAA in mammalian mRNA
744 3' processing. *Genes & development* 28, 2370-2380.

745 Chiu, A.C., Suzuki, H.I., Wu, X., Mahat, D.B., Kriz, A.J., and Sharp, P.A. (2018).
746 Transcriptional Pause Sites Delineate Stable Nucleosome-Associated Premature
747 Polyadenylation Suppressed by U1 snRNP. *Molecular cell* 69, 648-663 e647.

748 Cho, W.K., Spille, J.H., Hecht, M., Lee, C., Li, C., Grube, V., and Cisse, II (2018). Mediator
749 and RNA polymerase II clusters associate in transcription-dependent condensates. *Science*
750 361, 412-415.

751 Chung, H.K., Jacobs, C.L., Huo, Y., Yang, J., Krumm, S.A., Plemper, R.K., Tsien, R.Y., and
752 Lin, M.Z. (2015). Tunable and reversible drug control of protein production via a self-excising
753 degnon. *Nature chemical biology* 11, 713-720.

754 Clerici, M., Faini, M., Muckenfuss, L.M., Aebersold, R., and Jinek, M. (2018). Structural basis
755 of AAUAAA polyadenylation signal recognition by the human CPSF complex. *Nat Struct Mol*
756 *Biol* 25, 135-138.

757 Cortazar, M.A., Sheridan, R.M., Erickson, B., Fong, N., Glover-Cutter, K., Brannan, K., and
758 Bentley, D.L. (2019). Control of RNA Pol II Speed by PNUTS-PP1 and Spt5
759 Dephosphorylation Facilitates Termination by a "Sitting Duck Torpedo" Mechanism.
760 *Molecular cell*.

761 Davidson, L., Francis, L., Cordiner, R.A., Eaton, J.D., Estell, C., Macias, S., Caceres, J.F.,
762 and West, S. (2019). Rapid Depletion of DIS3, EXOSC10, or XRN2 Reveals the Immediate
763 Impact of Exoribonucleolysis on Nuclear RNA Metabolism and Transcriptional Control. *Cell*
764 *reports* 26, 2779-2791 e2775.

765 Davidson, L., Francis, L., Eaton, J.D., and West, S. (2020). Integrator-Dependent and
766 Allosteric/Intrinsic Mechanisms Ensure Efficient Termination of snRNA Transcription. *Cell*
767 *reports* 33, 108319.

- 768 Dubbury, S.J., Boutz, P.L., and Sharp, P.A. (2018). CDK12 regulates DNA repair genes by
769 suppressing intronic polyadenylation. *Nature* 564, 141-145.
- 770 Dye, M.J., Gromak, N., and Proudfoot, N.J. (2006). Exon tethering in transcription by RNA
771 polymerase II. *Molecular cell* 21, 849-859.
- 772 Eaton, J.D., Davidson, L., Bauer, D.L.V., Natsume, T., Kanemaki, M.T., and West, S. (2018).
773 Xrn2 accelerates termination by RNA polymerase II, which is underpinned by CPSF73
774 activity. *Genes & development* 32, 127-139.
- 775 Eaton, J.D., Francis, L., Davidson, L., and West, S. (2020). A unified allosteric/torpedo
776 mechanism for transcriptional termination on human protein-coding genes. *Genes &
777 development* 34, 132-145.
- 778 Eaton, J.D., and West, S. (2020). Termination of Transcription by RNA Polymerase II:
779 BOOM! *Trends Genet* 36, 664-675.
- 780 Eddy, S.R. (2011). Accelerated Profile HMM Searches. *PLoS Comput Biol* 7, e1002195.
- 781 Elrod, N.D., Henriques, T., Huang, K.L., Tatomer, D.C., Wilusz, J.E., Wagner, E.J., and
782 Adelman, K. (2019). The Integrator Complex Attenuates Promoter-Proximal Transcription at
783 Protein-Coding Genes. *Molecular cell* 76, 738-752 e737.
- 784 Fong, N., Brannan, K., Erickson, B., Kim, H., Cortazar, M.A., Sheridan, R.M., Nguyen, T.,
785 Karp, S., and Bentley, D.L. (2015). Effects of Transcription Elongation Rate and Xrn2
786 Exonuclease Activity on RNA Polymerase II Termination Suggest Widespread Kinetic
787 Competition. *Molecular cell* 60, 256-267.
- 788 Grant, C.E., Bailey, T.L., and Noble, W.S. (2011). FIMO: scanning for occurrences of a given
789 motif. *Bioinformatics* 27, 1017-1018.
- 790 Gregersen, L.H., Mitter, R., Ugalde, A.P., Nojima, T., Proudfoot, N.J., Agami, R., Stewart, A.,
791 and Svejstrup, J.Q. (2019). SCAF4 and SCAF8, mRNA Anti-Terminator Proteins. *Cell* 177,
792 1797-1813 e1718.
- 793 Hnisz, D., Abraham, B.J., Lee, T.I., Lau, A., Saint-Andre, V., Sigova, A.A., Hoke, H.A., and
794 Young, R.A. (2013). Super-enhancers in the control of cell identity and disease. *Cell* 155,
795 934-947.
- 796 Iasillo, C., Schmid, M., Yahia, Y., Maqbool, M.A., Descostes, N., Karadoulama, E., Bertrand,
797 E., Andrau, J.C., and Jensen, T.H. (2017). ARS2 is a general suppressor of pervasive
798 transcription. *Nucleic acids research* 45, 10229-10241.
- 799 Jensen, L.J., Kuhn, M., Stark, M., Chaffron, S., Creevey, C., Muller, J., Doerks, T., Julien, P.,
800 Roth, A., Simonovic, M., *et al.* (2009). STRING 8--a global view on proteins and their
801 functional interactions in 630 organisms. *Nucleic acids research* 37, D412-416.

802 Kaida, D., Berg, M.G., Younis, I., Kasim, M., Singh, L.N., Wan, L., and Dreyfuss, G. (2010).
803 U1 snRNP protects pre-mRNAs from premature cleavage and polyadenylation. *Nature* *468*,
804 664-668.

805 Kalyaanamoorthy, S., Minh, B.Q., Wong, T.K.F., von Haeseler, A., and Jermiin, L.S. (2017).
806 ModelFinder: fast model selection for accurate phylogenetic estimates. *Nat Methods* *14*,
807 587-589.

808 Kamieniarz-Gdula, K., Gdula, M.R., Panser, K., Nojima, T., Monks, J., Wisniewski, J.R.,
809 Riepsaame, J., Brockdorff, N., Pauli, A., and Proudfoot, N.J. (2019). Selective Roles of
810 Vertebrate PCF11 in Premature and Full-Length Transcript Termination. *Molecular cell* *74*,
811 158-172 e159.

812 Kamieniarz-Gdula, K., and Proudfoot, N.J. (2019). Transcriptional Control by Premature
813 Termination: A Forgotten Mechanism. *Trends Genet* *35*, 553-564.

814 Katoh, K., and Standley, D.M. (2013). MAFFT multiple sequence alignment software version
815 7: improvements in performance and usability. *Mol Biol Evol* *30*, 772-780.

816 Khan, A., and Zhang, X. (2016). dbSUPER: a database of super-enhancers in mouse and
817 human genome. *Nucleic acids research* *44*, D164-171.

818 Kieft, R., Zhang, Y., Marand, A.P., Moran, J.D., Bridger, R., Wells, L., Schmitz, R.J., and
819 Sabatini, R. (2020). Identification of a novel base J binding protein complex involved in RNA
820 polymerase II transcription termination in trypanosomes. *PLoS Genet* *16*, e1008390.

821 Kim, D., Langmead, B., and Salzberg, S.L. (2015). HISAT: a fast spliced aligner with low
822 memory requirements. *Nat Methods* *12*, 357-360.

823 Kopp, F., and Mendell, J.T. (2018). Functional Classification and Experimental Dissection of
824 Long Noncoding RNAs. *Cell* *172*, 393-407.

825 Kuan, Y.S., Brewer-Jensen, P., and Searles, L.L. (2004). Suppressor of sable, a putative
826 RNA-processing protein, functions at the level of transcription. *Molecular and cellular biology*
827 *24*, 3734-3746.

828 Kustatscher, G., Grabowski, P., Schrader, T.A., Passmore, J.B., Schrader, M., and
829 Rappsilber, J. (2019). Co-regulation map of the human proteome enables identification of
830 protein functions. *Nat Biotechnol* *37*, 1361-1371.

831 Lai, F., Gardini, A., Zhang, A., and Shiekhhattar, R. (2015). Integrator mediates the
832 biogenesis of enhancer RNAs. *Nature* *525*, 399-403.

833 Lee, J.H., and Skalnik, D.G. (2008). Wdr82 is a C-terminal domain-binding protein that
834 recruits the Setd1A Histone H3-Lys4 methyltransferase complex to transcription start sites of
835 transcribed human genes. *Molecular and cellular biology* *28*, 609-618.

836 Lee, J.H., You, J., Dobrota, E., and Skalnik, D.G. (2010). Identification and characterization
837 of a novel human PP1 phosphatase complex. *J Biol Chem* *285*, 24466-24476.

- 838 Letunic, I., and Bork, P. (2019). Interactive Tree Of Life (iTOL) v4: recent updates and new
839 developments. *Nucleic acids research* 47, W256-W259.
- 840 Li, H., Handsaker, B., Wysoker, A., Fennell, T., Ruan, J., Homer, N., Marth, G., Abecasis,
841 G., Durbin, R., and Genome Project Data Processing, S. (2009). The Sequence
842 Alignment/Map format and SAMtools. *Bioinformatics* 25, 2078-2079.
- 843 Liao, Y., Smyth, G.K., and Shi, W. (2013). The Subread aligner: fast, accurate and scalable
844 read mapping by seed-and-vote. *Nucleic acids research* 41, e108.
- 845 Liao, Y., Smyth, G.K., and Shi, W. (2014). featureCounts: an efficient general purpose
846 program for assigning sequence reads to genomic features. *Bioinformatics* 30, 923-930.
- 847 Love, M.I., Huber, W., and Anders, S. (2014). Moderated estimation of fold change and
848 dispersion for RNA-seq data with DESeq2. *Genome Biol* 15, 550.
- 849 Lykke-Andersen, S., Zumer, K., Molska, E.S., Rouviere, J.O., Wu, G., Demel, C., Schwalb,
850 B., Schmid, M., Cramer, P., and Jensen, T.H. (2020). Integrator is a genome-wide attenuator
851 of non-productive transcription. *Molecular cell*.
- 852 Manna, P.T., Davis, L.J., and Robinson, M.S. (2019). Fast and cloning-free CRISPR/Cas9-
853 mediated genomic editing in mammalian cells. *Traffic* 20, 974-982.
- 854 Mendoza-Figueroa, M.S., Tatomer, D.C., and Wilusz, J.E. (2020). The Integrator Complex in
855 Transcription and Development. *Trends Biochem Sci* 45, 923-934.
- 856 Mi, H., Muruganujan, A., Ebert, D., Huang, X., and Thomas, P.D. (2019). PANTHER version
857 14: more genomes, a new PANTHER GO-slim and improvements in enrichment analysis
858 tools. *Nucleic acids research* 47, D419-D426.
- 859 Minh, B.Q., Nguyen, M.A., and von Haeseler, A. (2013). Ultrafast approximation for
860 phylogenetic bootstrap. *Mol Biol Evol* 30, 1188-1195.
- 861 Natsume, T., Kiyomitsu, T., Saga, Y., and Kanemaki, M.T. (2016). Rapid Protein Depletion in
862 Human Cells by Auxin-Inducible Degron Tagging with Short Homology Donors. *Cell reports*
863 15, 210-218.
- 864 Nedea, E., He, X., Kim, M., Pootoolal, J., Zhong, G., Canadien, V., Hughes, T., Buratowski,
865 S., Moore, C.L., and Greenblatt, J. (2003). Organization and function of APT, a subcomplex
866 of the yeast cleavage and polyadenylation factor involved in the formation of mRNA and
867 small nucleolar RNA 3'-ends. *J Biol Chem* 278, 33000-33010.
- 868 Nguyen, L.T., Schmidt, H.A., von Haeseler, A., and Minh, B.Q. (2015). IQ-TREE: a fast and
869 effective stochastic algorithm for estimating maximum-likelihood phylogenies. *Mol Biol Evol*
870 32, 268-274.
- 871 Nojima, T., Gomes, T., Grosso, A.R.F., Kimura, H., Dye, M.J., Dhir, S., Carmo-Fonseca, M.,
872 and Proudfoot, N.J. (2015). Mammalian NET-Seq Reveals Genome-wide Nascent
873 Transcription Coupled to RNA Processing. *Cell* 161, 526-540.

874 Nojima, T., Tellier, M., Foxwell, J., Ribeiro de Almeida, C., Tan-Wong, S.M., Dhir, S.,
875 Dujardin, G., Dhir, A., Murphy, S., and Proudfoot, N.J. (2018). Deregulated Expression of
876 Mammalian lncRNA through Loss of SPT6 Induces R-Loop Formation, Replication Stress,
877 and Cellular Senescence. *Molecular cell* 72, 970-984 e977.

878 O'Reilly, D., Kuznetsova, O.V., Laitem, C., Zaborowska, J., Dienstbier, M., and Murphy, S.
879 (2014). Human snRNA genes use polyadenylation factors to promote efficient transcription
880 termination. *Nucleic acids research* 42, 264-275.

881 Oh, J.M., Di, C., Venters, C.C., Guo, J., Arai, C., So, B.R., Pinto, A.M., Zhang, Z., Wan, L.,
882 Younis, I., *et al.* (2017). U1 snRNP telescripting regulates a size-function-stratified human
883 genome. *Nat Struct Mol Biol* 24, 993-999.

884 Partridge, E.C., Chhetri, S.B., Prokop, J.W., Ramaker, R.C., Jansen, C.S., Goh, S.T.,
885 Mackiewicz, M., Newberry, K.M., Brandsmeier, L.A., Meadows, S.K., *et al.* (2020).
886 Occupancy maps of 208 chromatin-associated proteins in one human cell type. *Nature* 583,
887 720-728.

888 Pott, S., and Lieb, J.D. (2015). What are super-enhancers? *Nature genetics* 47, 8-12.

889 Preker, P., Nielsen, J., Kammler, S., Lykke-Andersen, S., Christensen, M.S., Mapendano,
890 C.K., Schierup, M.H., and Jensen, T.H. (2008). RNA exosome depletion reveals transcription
891 upstream of active human promoters. *Science* 322, 1851-1854.

892 Proudfoot, N.J. (2011). Ending the message: poly(A) signals then and now. *Genes &*
893 *development* 25, 1770-1782.

894 Quinlan, A.R., and Hall, I.M. (2010). BEDTools: a flexible suite of utilities for comparing
895 genomic features. *Bioinformatics* 26, 841-842.

896 Ramirez, F., Dundar, F., Diehl, S., Gruning, B.A., and Manke, T. (2014). deepTools: a
897 flexible platform for exploring deep-sequencing data. *Nucleic acids research* 42, W187-191.

898 Robert, X., and Gouet, P. (2014). Deciphering key features in protein structures with the new
899 ENDscript server. *Nucleic acids research* 42, W320-324.

900 Robinson, J.T., Thorvaldsdottir, H., Winckler, W., Guttman, M., Lander, E.S., Getz, G., and
901 Mesirov, J.P. (2011). Integrative genomics viewer. *Nat Biotechnol* 29, 24-26.

902 Sabari, B.R., Dall'Agnese, A., Bojja, A., Klein, I.A., Coffey, E.L., Shrinivas, K., Abraham, B.J.,
903 Hannett, N.M., Zamudio, A.V., Manteiga, J.C., *et al.* (2018). Coactivator condensation at
904 super-enhancers links phase separation and gene control. *Science* 361.

905 Schlackow, M., Nojima, T., Gomes, T., Dhir, A., Carmo-Fonseca, M., and Proudfoot, N.J.
906 (2017). Distinctive Patterns of Transcription and RNA Processing for Human lincRNAs.
907 *Molecular cell* 65, 25-38.

908 Sheridan, R.M., and Bentley, D.L. (2016). Selectable one-step PCR-mediated integration of
909 a degron for rapid depletion of endogenous human proteins. *Biotechniques* 60, 69-74.

910 Sun, Y., Zhang, Y., Hamilton, K., Manley, J.L., Shi, Y., Walz, T., and Tong, L. (2018).
911 Molecular basis for the recognition of the human AAUAAA polyadenylation signal.
912 Proceedings of the National Academy of Sciences of the United States of America 115,
913 E1419-E1428.

914 Tatomer, D.C., Elrod, N.D., Liang, D., Xiao, M.S., Jiang, J.Z., Jonathan, M., Huang, K.L.,
915 Wagner, E.J., Cherry, S., and Wilusz, J.E. (2019). The Integrator complex cleaves nascent
916 mRNAs to attenuate transcription. Genes & development 33, 1525-1538.

917 Trendel, J., Schwarzl, T., Horos, R., Prakash, A., Bateman, A., Hentze, M.W., and
918 Krijgsveld, J. (2019). The Human RNA-Binding Proteome and Its Dynamics during
919 Translational Arrest. Cell 176, 391-403 e319.

920 van Nuland, R., Smits, A.H., Pallaki, P., Jansen, P.W., Vermeulen, M., and Timmers, H.T.
921 (2013). Quantitative dissection and stoichiometry determination of the human SET1/MLL
922 histone methyltransferase complexes. Molecular and cellular biology 33, 2067-2077.

923 Wuarin, J., and Schibler, U. (1994). Physical isolation of nascent RNA chains transcribed by
924 RNA polymerase II: evidence for cotranscriptional splicing. Molecular and cellular biology 14,
925 7219-7225.

926 Yu, G., Wang, L.G., and He, Q.Y. (2015). ChIPseeker: an R/Bioconductor package for ChIP
927 peak annotation, comparison and visualization. Bioinformatics 31, 2382-2383.

928 Zhang, Y., Liu, T., Meyer, C.A., Eeckhoute, J., Johnson, D.S., Bernstein, B.E., Nusbaum, C.,
929 Myers, R.M., Brown, M., Li, W., et al. (2008). Model-based analysis of ChIP-Seq (MACS).
930 Genome Biol 9, R137.

931

932 **FIGURE LEGENDS**

933 **Figure 1: Proximity labelling of CPSF30-sensitive Pol II interactions by mTurbo**

934 a) Schematic of the strategy used to tag CPSF30 with the mini auxin-inducible degron
935 (mAID). Guide RNA-expressing Cas9 plasmid and homology-directed repair (HDR) plasmids
936 are shown and the resulting modification to *CPSF30* is represented with each inserted
937 element labelled.

938 b) Western blot demonstrating CPSF30 depletion. Parental HCT116-TIR1, or *CPSF30-mAID*
939 cells, were treated +/- auxin for 3 hours then blotted. CPSF30 protein is indicated together
940 with a non-specific product, marked by an asterisk, used as a proxy for protein loading.

941 c) Metagene analysis of 1795 protein-coding genes demonstrating increased downstream
942 transcription, derived from sequencing nuclear RNA, following auxin treatment (3hr) of
943 *CPSF30-mAID* cells. TSS = transcription start site, TES = transcription end site (PAS), read-
944 through signal is normalised against gene body. RPKM is Reads Per Kilobase of transcript,

945 per Million mapped reads. Positive and negative signals represent sense and antisense
946 reads, respectively.

947 d) Schematic of our strategy to identify new factors involved in transcription termination.
948 *CPSF30-mAID* cells edited to contain Rpb1-mTurbo (blue circle on Pol II). The addition of
949 biotin induces mTurbo-mediated biotinylation (orange haze) of factors proximal to Pol II.
950 CPSF complex is shown as an example of what might be captured by this experiment.

951 e) Western blot showing streptavidin HRP probing of extracts from *CPSF30-mAID: RPB1-*
952 *mTurbo* cells. Prior treatment with auxin (3hr)/biotin (10 mins) is indicated. The high
953 molecular weight species in the + biotin samples corresponds in size to Rpb1-mTurbo (*).

954 f) Heat map detailing proteins with the largest decrease in Pol II interaction. Data
955 underpinning heat map are from mass spectrometry analysis of streptavidin sequestered
956 peptides (+/- CPSF30) performed in triplicate. Labelling was for 10 minutes.

957

958 **Figure 2: ZC3H4 depletion stabilises unproductive transcripts.**

959 a) IGV track of the transcription read-through defect at *PTPN11* following CPSF30 or ZC3H4
960 depletion. Blue and red tracks indicate sense/anti-sense transcripts respectively, grey bar
961 indicates a change in y-axis scale so that comparatively weaker read-through signals can be
962 visualised next to the gene body (left scale for upstream of TES; right for downstream). Y-
963 axis scale is RPKM.

964 b) Metagene comparison of transcription upstream, across, and downstream of, protein-
965 coding genes in nuclear RNA from *CPSF30-mAID* cells treated or not with auxin and from
966 HCT116 cells transfected with control or ZC3H4 siRNAs. CPSF30 traces are from the same
967 samples presented in Figure 1C. Positive and negative signals represent sense and
968 antisense reads, respectively.

969 c) IGV track view of transcription at the *MYC* PROMPT in RNA-seq samples obtained from
970 control or ZC3H4 siRNA treated HCT116 cells. We also show a track from HCT116 cells
971 acutely depleted of DIS3-AID (DIS3 +IAA) (Davidson et al., 2019) to highlight the normal
972 extent of this unstable transcript. Y-axis scale is RPKM.

973 d) Log₂ fold change of siZC3H4 vs siControl or DIS3 + vs - auxin for RNA upstream of 6057
974 non-neighbouring, actively transcribed genes, plotted as heat maps. Line graphs are an XY
975 depiction of heat map data. Log₂ fold changes are smaller in siZC3H4 samples versus DIS3
976 depletion because this is an average of all genes in the heat map, a smaller fraction of which
977 are affected by ZC3H4.

978 e) IGV plot of a known SE upstream of *MYC* (the location is shown by blue bar under trace).
979 Samples are shown from HCT116 cells treated with control or ZC3H4 siRNAs as well as
980 *DIS3-AID* cells treated with auxin (the latter from (Davidson et al., 2019)) to show the normal
981 extent of unstable eRNAs over this region. Y-axis scale is RPKM.

982 f) Log2 fold change of RNA signal for siZC3H4 vs siControl or DIS3 + vs - auxin for 111 SEs.
983 The bed file detailing super-enhancer coordinates in HCT116 cells was taken from
984 dbSUPER.org.

985

986 **Figure 3: Comparison of ZC3H4 and Integrator effects**

987 a) Metagene analysis of chromatin-associated RNA-seq performed on cells treated with
988 control or INTS1-specific siRNA. The plot shows signals upstream, across and downstream
989 of protein-coding genes. Y-axis scale is RPKM. Positive and negative values represent
990 sense and antisense reads, respectively.

991 b/c) IGV traces of *HAP1* and *NWD1* genes derived from chromatin-associated RNA-seq in
992 control and INTS1 siRNA treated samples and nuclear RNA-seq from control or ZC3H4
993 siRNA treatment. *NWD1* transcripts are affected by ZC3H4 but not INTS1 whereas the
994 opposite is true for *HAP1* RNAs. Y-axes scales are RPKM.

995 d) Venn diagram showing the number of mRNAs upregulated ≥ 2 -fold, $\text{padj} \leq 0.05$ following
996 ZC3H4 depletion versus INTS1 loss and the overlap between the two sets. Genes that
997 showed increased expression due to transcription read-through from an upstream gene were
998 also discarded by assessing coverage over a 1 kb region preceding the TSS, relative to
999 untreated cells. Gene lists are provided in Supplemental File 3.

1000 e) Graphs demonstrating the expression level of mRNA transcripts upregulated ($\log_2\text{FC} > 1$)
1001 following ZC3H4 or INTS1 depletion by comparison with transcripts unaffected by loss of
1002 either factor. Y-axis shows normalised gene counts (i.e. expression level).

1003 f) Comparison of chromatin-associated RNA-seq in control and INTS1 siRNA treated
1004 samples with nuclear RNA-seq derived from control or ZC3H4 siRNA treatment. The
1005 *ITPRID2* PROMPT is displayed and y-axes are RPKM (note the different scales between
1006 ZC3H4 and INTS1 samples).

1007 g) Comparison of chromatin-associated RNA-seq in control and INTS1 siRNA treated
1008 samples with nuclear RNA-seq derived from control or ZC3H4 siRNA treatment. The
1009 *MSRB3* SE is displayed and y-axes are RPKM (note the different scales between INTS1 and
1010 ZC3H4 samples).

1011 h) Metaplot of RNA-seq profile over super-enhancers following INTS1 depletion (log₂ fold
1012 depletion/control over 111 super-enhancer as line graphs). The bed file detailing super-
1013 enhancer coordinates in HCT116 cells was taken from dbSUPER.org.

1014

1015 **Figure 4: Transcriptional dysregulation following acute ZC3H4 loss.**

1016 a) Schematic detailing how the DHFR degron works. *E. Coli* dihydrofolate reductase (DHFR)
1017 is fused to the C-terminus of ZC3H4, which is stabilised by trimethoprim (TMP). When TMP
1018 is removed ZC3H4-DHFR is degraded.

1019 b) Western blot of HCT116 parental and HCT116 *ZC3H4-DHFR* cells +/- TMP. TMP was
1020 withdrawn for 4 hours or overnight, EXOSC10 is used as a loading control, αHA recognises
1021 a HA peptide before the DHFR tag, while αZC3H4 recognises native protein.

1022 c) Western blot of *ZC3H4-DHFR* cells grown under the following conditions: +TMP, -TMP
1023 (4hr), -TMP (4hr) followed by +TMP (4hr). ZC3H4-DHFR is detected using αHA and
1024 EXOSC10 is shown as a loading control.

1025 d) qRT-PCR analysis of PROMPT and SE transcripts in *ZC3H4-DHFR* cells grown under the
1026 conditions represented in c) (rescue refers to -TMP then +TMP for re-establishing ZC3H4).
1027 Graph shows fold change versus +TMP following normalisation to spliced actin. N=3. Error
1028 bars are standard error of the mean (SEM). *, ** and *** denote p values of <0.05, 0.01 and
1029 0.001 respectively. ITPRID2 5' and 3' primers are at approximately -500bp and -7kb relative
1030 to its TSS. HMGA2 5' and 3' primers are at approximately -1.8kb and -7.1kb relative to its
1031 TSS.

1032 e) qRT-PCR analysis of spliced PJVK, ENO3 and NWD1 mRNAs and RNU1-1 read-through
1033 (RT) in *ZC3H4-DHFR* cells grown with or without (4hr) TMP and *INTS11-SMASH* cells grown
1034 with or without asunaprevir (ASN; 36 hrs). Graph shows fold change versus control (+TMP
1035 for ZC3H4-DHFR samples and -ASN for INTS11-SMASH samples), following normalisation
1036 to spliced actin. N=3. Error bars are SEM. * and ** denote p values of <0.05 and 0.01
1037 respectively.

1038 f) Western blot of extracts derived from HCT116 cells transfected with control or WDR82-
1039 specific siRNAs. The blot shows WDR82 and, as a loading control, EXOSC10.

1040 g) qRT-PCR of PROMPT and SE transcripts in *ZC3H4-DHFR* cells transfected with control
1041 or WDR82 siRNAs before withdrawal, or not, of TMP (14hr). Graph shows fold change by
1042 comparison with control siRNA transfected *ZC3H4-DHFR* cells maintained in TMP following

1043 normalisation to spliced actin transcripts. N=3. Error bars are SEM. * and ** denote $p < 0.05$
1044 and 0.01, respectively.

1045

1046 **Figure 5: ZC3H4 occupies regions where transcription is affected by its absence.**

1047 a) ZC3H4 ChIP profile over protein-coding genes is similar to Pol II. Heat map
1048 representation of ZC3H4 and Pol II ChIP-seq occupancy over the gene body +/- 3 kb.

1049 b) ZC3H4 occupies fewer promoters than Pol II. IGV track view of ZC3H4 and Pol II
1050 occupancy over *KAZALD1* and *FABP5* genes, Pol II is present at both genes, while ZC3H4
1051 is only present at *KAZALD1*. Scale is counts per million (CPM). Shaded blue box shows
1052 peak of Pol II and ZC3H4 at *KAZALD1* and of Pol II over *FABP5*.

1053 c) RNA-seq (HCT116 cells treated with control or ZC3H4 siRNA) and ChIP-seq (Pol II,
1054 ZC3H4 and input) profiles at *RPL13*. ZC3H4 occupancy is focused more on the PROMPT
1055 transcript region (blue box) than the TSS where, in contrast, the Pol II signal is maximal.
1056 RNA-seq scale is RPKM and ChIP-seq is CPM.

1057 d) ZC3H4 ChIP occupancy mirrors Pol II at super-enhancers. IGV track view of ZC3H4 and
1058 Pol II occupancy over the SE at the *MSRB3* locus. HCT116 super-enhancer gene track is
1059 from dbSUPER and depicted as blue bars.

1060 e) Log2 fold change of ZC3H4 and Pol II vs input at SEs shown as a line graph. Halo
1061 denotes 95% confidence level.

1062 f) ChIPseeker analysis of peak distribution of ZC3H4 and Pol II. Occupancy regions are
1063 colour-coded and the number of ChIP peaks expressed as a proportion of 100%.

1064 g) Heat map showing Pol II and ZC3H4 ChIP occupancy in HEPG2 cells obtained via the
1065 ENCODE consortium. Occupancy +/- 2 kb of the TSS is shown.

1066

1067 **Figure 6: Directed recruitment of ZC3H4 recapitulates its effects on endogenous**
1068 **targets**

1069 a) Schematic of the MS2 system. A reporter plasmid (MS2hp-IRES-GFP) expressing a GFP
1070 transcript with 6 x MS2 hairpins upstream of an IRES and GFP gene. ZC3H4-MS2 or MS2-
1071 GFP can be specifically tethered to the MS2 hairpins to assess consequent effects on
1072 transcription/RNA output. Positions of primer pairs used in qRT-PCR experiments
1073 elsewhere in the figure are indicated by labelled horizontal lines under reporter. POI is
1074 protein of interest.

1075 b) qRT-PCR analysis of total RNA isolated from MS2hp-IRES-GFP transfected cells co-
1076 transfected with either MS2-GFP, ZC3H4-GFP or ZC3H4-MS2. The level of reporter RNA is
1077 plotted (“UP” amplicon) as a percentage of that obtained in the MS2-GFP sample following
1078 normalisation to spliced actin. N=3. Error bars are SEM. * denotes $p < 0.05$.

1079 c) qRT-PCR analysis of chromatin-associated RNA isolated from MS2hp-IRES-GFP
1080 transfected cells co-transfected with either MS2-GFP or ZC3H4-MS2. The level of reporter
1081 RNA upstream of the MS2 hairpins (UP) and transcripts yet to be cleaved at the BGH
1082 poly(A) site (BGH UC) are plotted as a percentage of that obtained in the MS2-GFP sample
1083 following normalisation to spliced actin. N=3. Error bars are SEM. * denotes $p < 0.05$.

1084 d) qRT-PCR analysis of total RNA isolated from MS2hp-IRES-GFP transfected *DIS3-AID*
1085 cells co-transfected with either MS2-GFP or ZC3H4-MS2 – simultaneously treated or not
1086 with auxin (14hr in total). The graph shows the ratio of RNA species recovered upstream
1087 (UP) versus downstream (DOWN) of the MS2 hairpins. N=4. Error bars are SEM. * denotes
1088 $p < 0.05$.

1089 e) Schematic detailing an interplay between ZC3H4 and DIS3 that sees transcription stop
1090 and nascent RNA degraded

1091 f) Colony formation assay of *ZC3H4-DHFR* cells grown in the presence or absence of TMP.
1092 Cells were grown for 10 days before crystal violet staining.

1093

1094 **SUPPLEMENTAL FIGURE LEGENDS**

1095 **Figure 1 – figure supplement 1**

1096 a) IGV track views of the transcription termination defect at *PCBP1*, *PSMC2*, *LSM8* and
1097 *CAV2* genes in the presence (CPSF30-IAA) or absence of (CPSF30 +IAA) in *CPSF30-mAID*
1098 cells. Signal is RPKM.

1099 b) Western blot demonstrating bi-allelic modification of RPB1 (Pol II) with mTurbo. The
1100 clone employed in Figure 1 is shown against cells parental HCT116 cells unmodified at
1101 *RBP1*. The upshift of Pol II signal shows the bi-allelic modification of RPB1. EXOSC10
1102 serves as a loading control.

1103 c) qRT-PCR of total RNA isolated from *CPSF30-mAID: RPB1- mTurbo* cells treated or not
1104 with auxin (3hr). An amplicon located ~10kb downstream of the *HMGA2* PAS was used to
1105 assay transcriptional read-through presented as a fold change versus minus auxin after
1106 normalising to spliced actin mRNA. n=2. Individual data points are shown.

1107

1108 **Figure 1 – figure supplement 2**

1109 a) Schematic of ZC3H4 and ZC3H6 showing the three CCCH zinc finger domains. A
1110 predictor of natural disordered region (PONDR) analysis shows that the only ordered region
1111 coincides with these domains. Graph generated via PONDR.com, set to VSL2.

1112 b) STRING analysis of ZC3H4 and ZC3H6 indicate interactors with 3' end processing
1113 complex. Image was taken from string.db.org, confidence value was set to medium (0.4).
1114 The thickness of lines between nodes is indicative of the confidence in interaction.

1115 c) Proteins that are co-regulated with ZC3H4 according to ProteomeHD using a score cut-off
1116 set to 0.98. Table shows GO term analysis of the potentially co-regulated factors.

1117 d) Co-immunoprecipitation of WDR82 using ZC3H4-GFP as bait. Blot shows input (5%) and
1118 immunoprecipitated material probed with antibodies to WDR82 or GFP. Cells untransfected
1119 with ZC3H4-GFP act as a negative control.

1120

1121 **Figure 1 – figure supplement 3**

1122 a) Maximum-likelihood phylogenetic tree of zinc finger CCCH-domains (1513 sequences;
1123 795 parsimony informative sites) inferred under the JTT+R8 model. Clades of ZC3H4-like
1124 and 845 ZC3H6-like domains are delimited by dashed lines. CCCH-domains identified using
1125 the PANTHER hidden Markov model PTHR13119 against the UniProtKB protein database
1126 (non redundant version: UniRef100; external node size represents protein cluster size).
1127 Branch support values $\geq 90\%$ (based on 1000 ultrafast bootstraps) are indicated by grey
1128 circles. Red stars show SwissProt reviewed protein sequences; external nodes are color-
1129 coded according to their taxonomic lineage. Scale bar represents the number of estimated
1130 substitutions per site. Virtually all recovered sequences were from metazoan organisms—
1131 except for a group of fungal sequences from ascomycetes. The resulting phylogenetic tree
1132 shows the dichotomy between the ZC3H4 and ZC3H6 domains, which are found in the same
1133 set of organisms. This indicates that they are paralogues and have likely diverged their
1134 function following gene duplication. The ancestral gene coding for ZC3H4/6 was likely lost
1135 from the non-vertebrates and subsequently underwent a duplication event leading to the
1136 ZC3H4- and ZC3H6-like paralogues in vertebrates. Primary data are available in
1137 Supplementary File 2 and deposited at Zenodo (<https://doi.org/10.5281/zenodo.4637127>).

1138 b) Multiple sequence alignment of ZC3H4 and ZC3H6 homologs. PTHR13119 domains from
1139 human and mouse SwissProt sequences were aligned using structural information (PDB

1140 structure: 2CQE; zinc-finger domain; helices are displayed as coils) using TCoffee (Expresso
1141 mode). Conserved regions are indicated by blue boxes; identical and similar residues (based
1142 on physicochemical properties) are marked in red and yellow, respectively. Sequence
1143 identifiers correspond to UniProt/SwissProt accession numbers and to boundaries of
1144 identified PTHR13119 domains. Alignment figure was rendered with ESPscript.

1145

1146 **Figure 2 – figure supplement 1**

1147 a) qRT-PCR and western blotting evidence of the effectiveness of ZC3H6 and ZC3H4
1148 depletion respectively. Graph shows fold reduction of ZC3H6 mRNA in cells treated with
1149 ZC3H6 siRNAs versus those transfected with control siRNA. N=3, error bars are SEM. ** is
1150 $p < 0.01$. Western blotting of ZC3H4 in HCT116 cells treated with control siRNAs or ZC3H4-
1151 targeting siRNAs. The blot was probed with a ZC3H4 antibody revealing strong depletion
1152 versus the EXOSC10 loading control.

1153 b) Pearson's correlation of siControl, siZC3H4, siZC3H6 and siZC3H4+6 of RNAseq BAM
1154 files performed by DEEPTOOLS.

1155 c) IGV traces exemplifying two genomic regions with clear RNA accumulation following
1156 ZC3H4 depletion. While this is also seen following ZC3H4/ZC3H6 co-depletion, it is not
1157 evident following the depletion of ZC3H6 alone. This was generally seen, supporting the
1158 correlation analysis in b). y-axis scale is RPKM.

1159

1160 **Figure 2 – figure supplement 2**

1161 a) Heatmaps showing the effects of CPSF30-mAID or ZC3H4 depletion on read-through
1162 beyond protein-coding genes. Coloured scale bar indicates the magnitude of effect (log2
1163 scale). Read-through was scored as a ratio of reads upstream (500bp) and downstream
1164 (1kb) of the PAS. The lists associated with this heatmap are provided in Supplementary File
1165 3.

1166 b) Graph showing the number of protein-coding genes with read-through enhancements of
1167 greater than 0.5, 1, 2 or 3 on a log2 fold scale. This illustrates that the effects of CPSF30-
1168 mAID loss are both wider spread and larger than those associated with depletion of ZC3H4.

1169 c) Venn diagram showing the number of genes bioinformatically scored as having increased
1170 read-through (log2 fold of 1 or more) following CPSF30-mAID or ZC3H4 loss and those that
1171 are common between the two conditions.

1172 d) IGV tracks of individual genes (*MAGED1* and *DLG3*) to exemplify the lack of 3'
1173 termination defect following ZC3H4 depletion. As a control for *bone fide* read-through, the
1174 same tracks are shown in samples obtained from *CPSF30-mAID* cells treated or not (3hr)
1175 with auxin. Grey bar indicates a change in scale (left scale for upstream of PAS; right for
1176 downstream) so that comparatively weaker read-through signals can be visualised next to
1177 the gene body. y-axis scale is RPKM.

1178 e) CPSF30 depletion shows little effect at super-enhancers and PROMPTs. IGV track view
1179 of the *MYC* super-enhancer and PROMPT in RNA-seq data obtained from *CPSF30-mAID*
1180 cells treated or not (3hr) with auxin. y-axis scale is RPKM.

1181 f) Plot showing the density of PAS sequences (AWTAAA) in PROMPTs upregulated or
1182 unaffected by ZC3H4 loss. Y-axis plots number of PAS sequences/kb.

1183 **Figure 3 – figure supplement 1**

1184 a) IGV snapshots showing examples of protein-coding genes selectively upregulated by
1185 ZC3H4 (*PJVK* and *ENO3*) or Integrator (*TM7SF2* and *GFPT2*). Y-axis represents RPKM.

1186 b) Venn diagram showing representing the number of protein-coding transcripts (determined
1187 by DESEQ2) that show increased levels in previously published 4sU labelling experiments
1188 performed on HeLa cells depleted of INTS11 or ZC3H4 (Austena et al., 2021; Lykke-
1189 Andersen et al., 2020). Gene lists are provided in Supplementary File 5. Notably, manual
1190 curation of this list revealed the presence of false positive hits, especially in the INTS11 data,
1191 due to DESEQ2 scoring interference of transcription from neighbouring genes as
1192 upregulation.

1193 c) Venn diagram showing the number of PROMPTs showing upregulation (log₂ fold of 1 or
1194 more) following ZC3H4 or INTS1 loss from HCT116 cells and those that are common
1195 between the two conditions.

1196 d) Graph showing the number of PROMPTs enhanced by greater than 0.5, 1, 2 or 3 on a
1197 log₂ fold scale following the loss of ZC3H4 or INTS1. This illustrates that the effects of
1198 ZC3H4 loss are both wider spread and larger than those associated with depletion of INTS1.
1199 The list of targets in each case is provided in Supplementary File 6.

1200

1201 **Figure 4 – figure supplement 1**

1202 a) Pol II ChIP over *ITPRID2* and *MYC* PROMPT regions. Graphs plot Pol II occupancy as a
1203 percentage of input at amplicons ~2, 4 and 8kb upstream of each gene. N=4. Error bars are

1204 SEM. * denotes p of <0.05. The schematic illustrates the approximate location of each
1205 primer pair.

1206 b) qRT-PCR analysis of extended ITPRID2 and MYC PROMPTs (-8kb amplicons) in
1207 chromatin-associated RNA isolated from *ZC3H4-DHFR* cells grown with or without (4hr)
1208 TMP. Y-axis displays fold change versus +TMP following normalisation to spliced actin
1209 levels. n=3. Error bars are SEM. * and ** denote p values of <0.05 and 0.01 respectively.

1210 c) Western blot showing acute depletion of PNUTS (the nuclear targeting subunit of PP1
1211 phosphatase), tagged with an auxin-inducible degron (PNUTS-AID). Blot shows extracts
1212 from unmodified HCT116 cells and *PNUTS-AID* cells which were treated or not with auxin
1213 (3hr). WDR82 is used as a loading control.

1214 d) qRT-PCR of PROMPT and SE transcripts in *PNUTS-AID* cells treated or not with auxin (3
1215 hr). Graph shows fold change by comparison with non-auxin treated cells following
1216 normalisation to spliced actin transcripts. N=3. Error bars are SEM. * and ** denote p
1217 values of <0.05 and 0.01 respectively.

1218 e) qRT-PCR analysis of PROMPT and SE transcripts in HCT116 cells treated with control
1219 siRNAs or siRNAs against both SETD1A and B. Quantitation shows fold change versus
1220 cells transfected with control siRNAs following normalisation to spliced actin levels. Note
1221 that the PROMPT and SE targets that are increased following ZC3H4 loss show relatively
1222 little change following depletion of SETD1A and B. The success of the RNAi is indicated by
1223 the strong reduction of SETD1A and B mRNAs. N=3. Error bars show SEM. ** denotes p
1224 value of <0.01.

1225 **Figure 5 – figure supplement 1**

1226 a) XRNAX analysis of ZC3H4 RNA binding in cells. Samples show input and those isolated
1227 following UV treatment or not. Bands representing each protein are labelled accordingly.
1228 ZC3H4 is recovered in a UV-dependent manner indicating that it is directly bound to RNA in
1229 cells. The same is true of EXOSC10 that, as an exoribonuclease, acts as a positive control.
1230 TCF4 is a DNA binding transcription factor and acts as a negative control.

1231 b) ZC3H4 only marks transcribed super-enhancers. IGV track view of ZC3H4 and Pol II
1232 occupancy at two different super-enhancers, *DLGAP1* present in both HEPG2 and
1233 HCT116 (top tracks) and the MYC super-enhancer (bottom tracks) that is only present in
1234 HCT116 cells. HEPG2 and HCT116 super-enhancer annotation is under each track as blue
1235 bars and was obtained from dbSUPER. Y-axis shows CPM.

1236 **Figure 6 – figure supplement 1**

1237 a) qRT-PCR of *ZC3H4-DHFR* cells transfected with MS2-IRES-GFP before growth in the
1238 presence or, to deplete ZC3H4, absence of TMP (4 hr). Graph shows percentage of each
1239 amplicon following TMP removal relative to that found in the presence of TMP following
1240 normalisation to spliced actin transcripts. N=3. Error bars show SEM. * denotes $p < 0.05$.

1241 b) qRT-PCR of HCT116 cells transfected with IRES-GFP and either a control beta-globin
1242 plasmid (NTC) or ZC3H4-MS2. The graph shows the percentage of GFP RNA versus
1243 control following normalisation to spliced actin transcripts. N=3. Error bars show SEM.

1244 **SUPPLEMENTARY FILES**

1245 **Supplementary File 1**

1246 Mass spectrometry data associated with the Pol II-miniTurbo experiment.

1247 **Supplementary File 2**

1248 Underpinning data for phylogenetic analyses.

1249 **Supplementary File 3**

1250 Log₂ fold changes in read-through following CPSF30 or ZC3H4 depletion from HCT116
1251 cells.

1252 **Supplementary File 4**

1253 List of mRNAs that are upregulated following ZC3H4 depletion (nuclear RNA-seq) or INTS1
1254 depletion (chromatin-associated RNA-seq) in HCT116 cells.

1255 **Supplementary File 5**

1256 List of mRNAs that are upregulated following ZC3H4 depletion (4sU RNA-seq; (Austena et
1257 al., 2021)) or INTS11 depletion (4sU TT-seq; (Lykke-Andersen et al., 2020)) in HeLa cells.
1258 Genes in each set were manually checked for upregulation (TRUE) or possible artefacts –
1259 primarily transcription from surrounding region into a gene that is consequently scored as
1260 upregulated (FALSE).

1261 **Supplementary File 6**

1262 List of PROMPTs that are upregulated following ZC3H4 depletion (nuclear RNA-seq) or
1263 INTS1 depletion (chromatin-associated RNA-seq) in HCT116 cells.

1264 **Supplementary File 7**

1265 Table of oligonucleotide and DNA sequences used in this study.

1266 **Source data file 1**

1267 Values (average, SEM, p-value) of data underpinning graphs within the paper.

1268 **Source data file 2**

1269 Uncropped western blot images.

1270

1271

1272

1273

1274

Figure 1

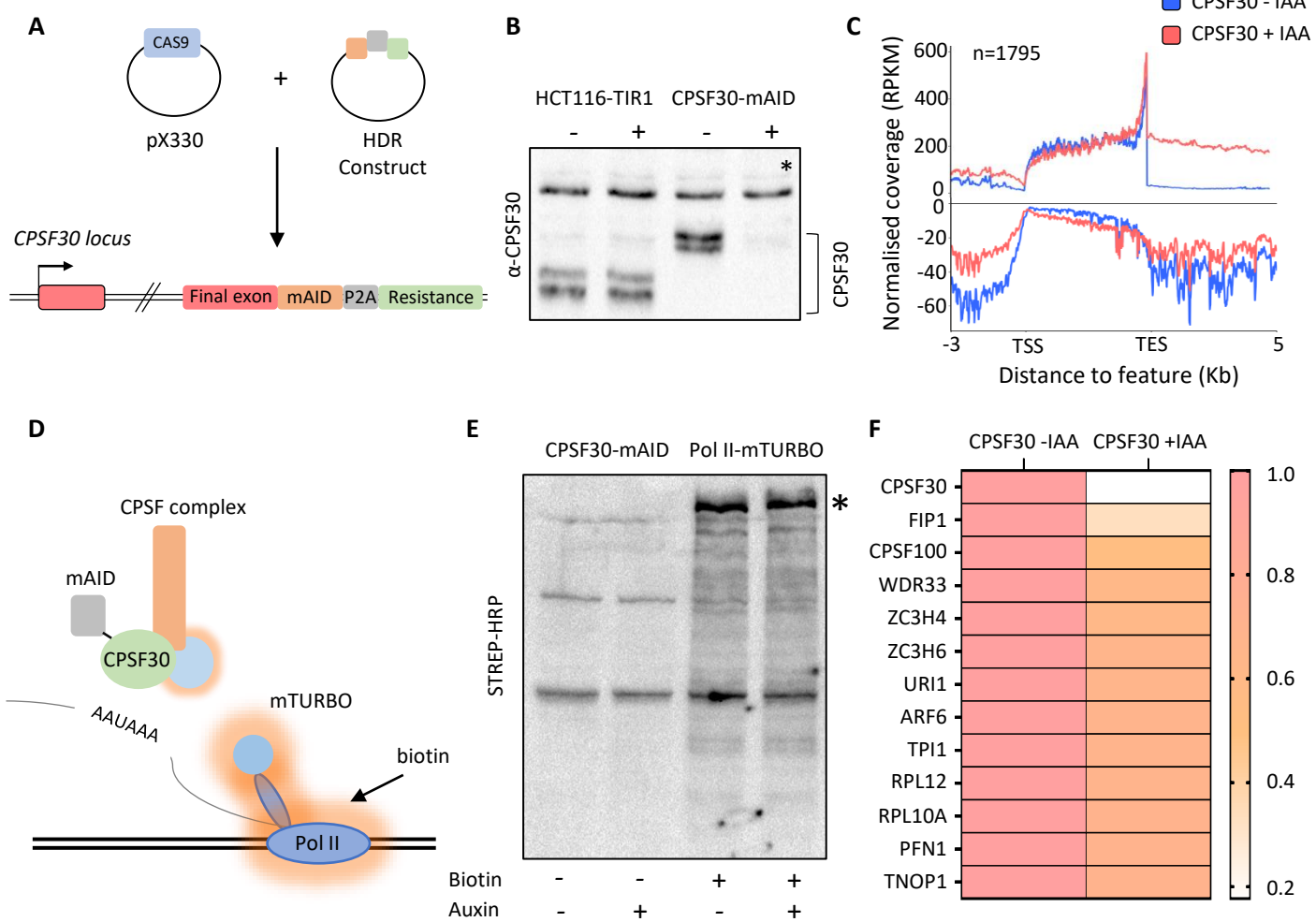


Figure 2

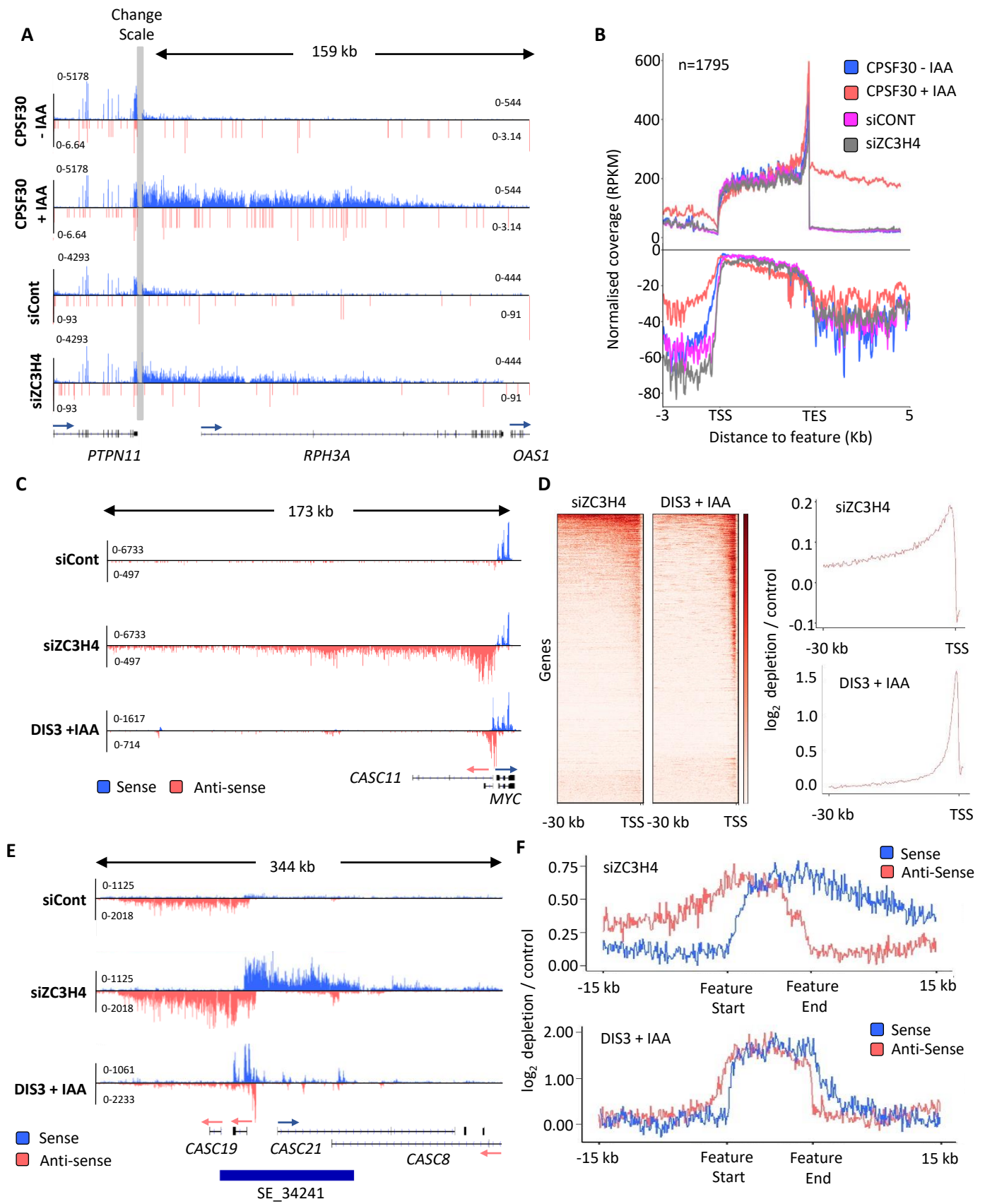


Figure 3

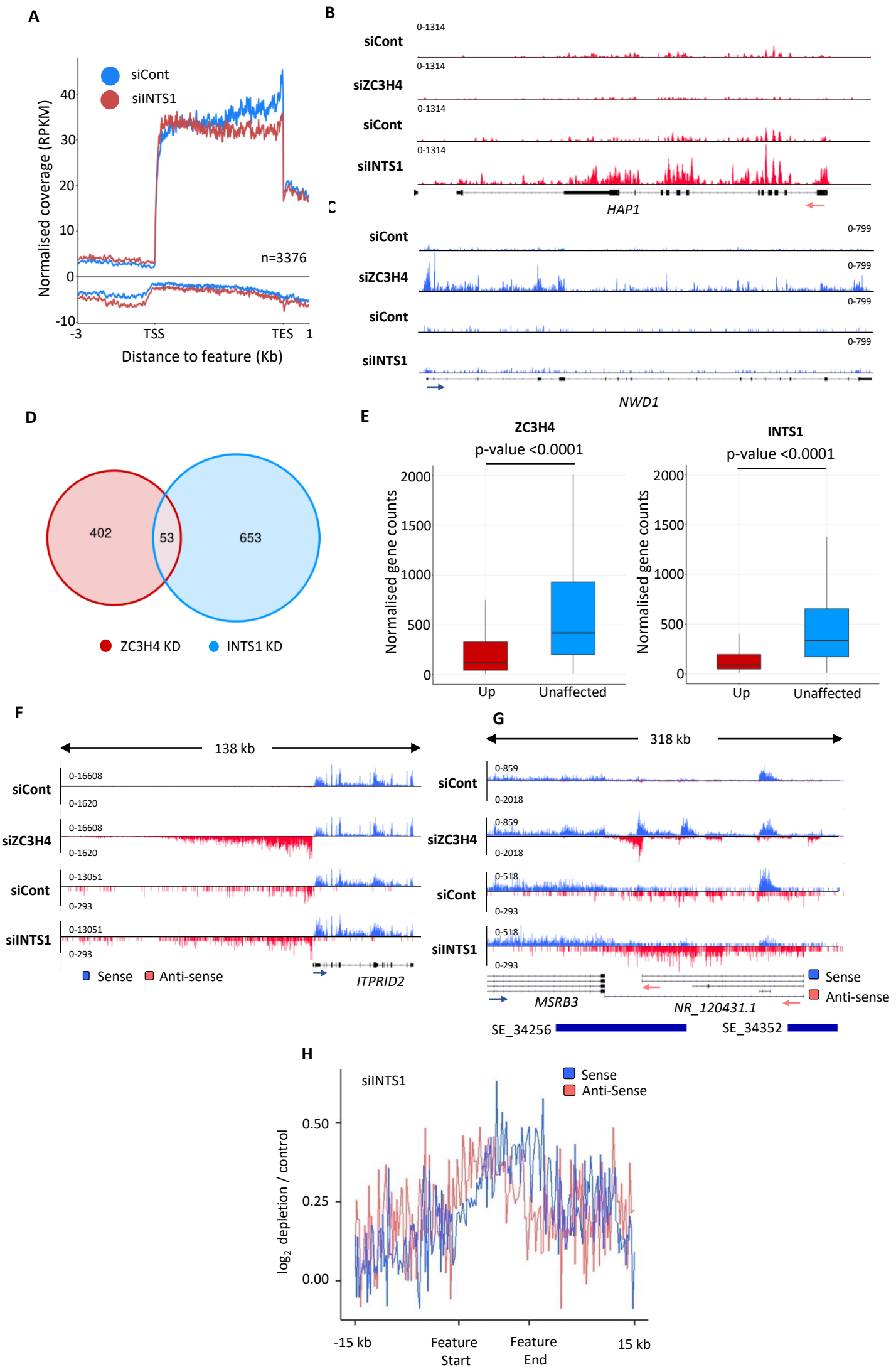


Figure 4

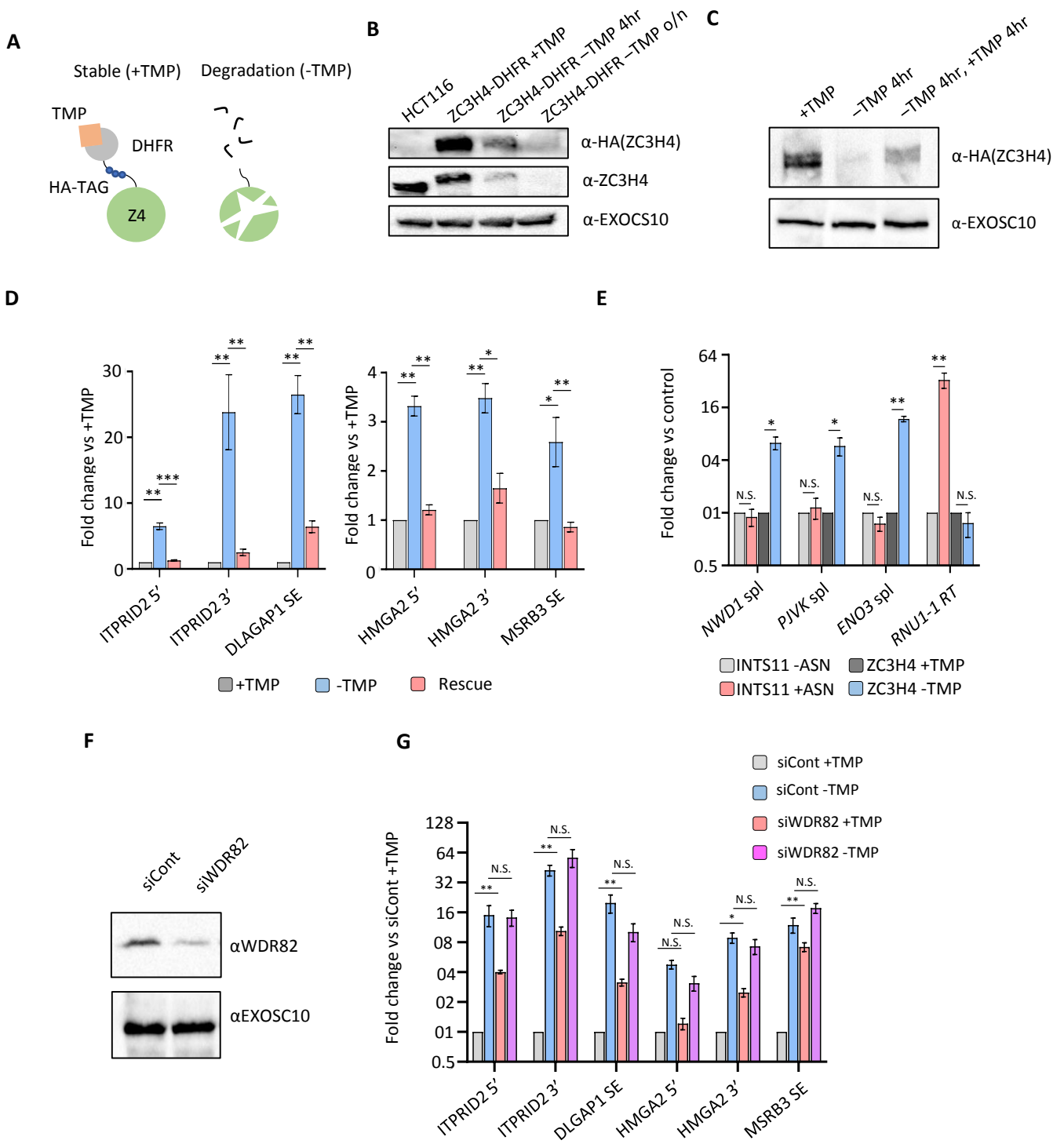


Figure 5

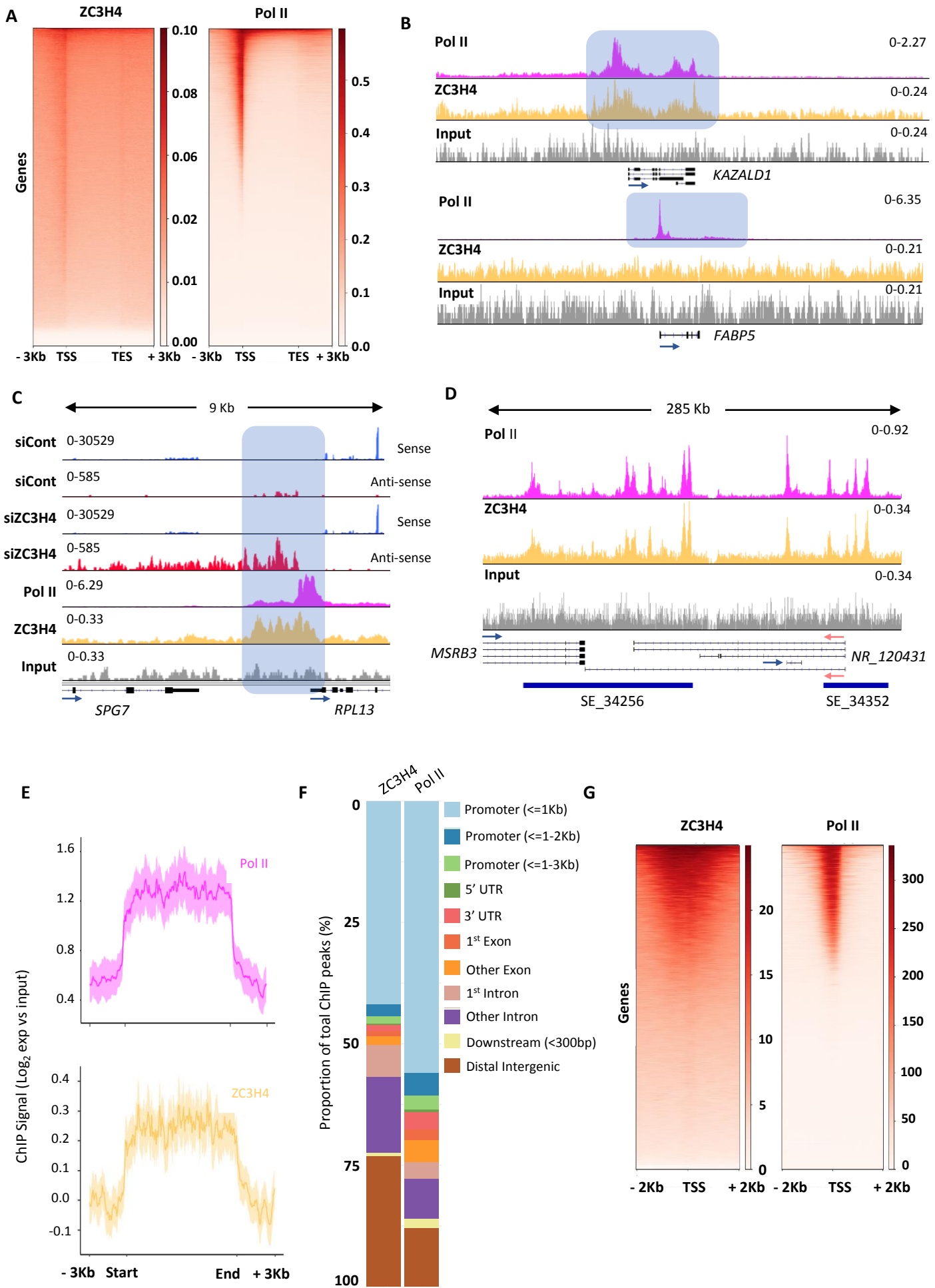
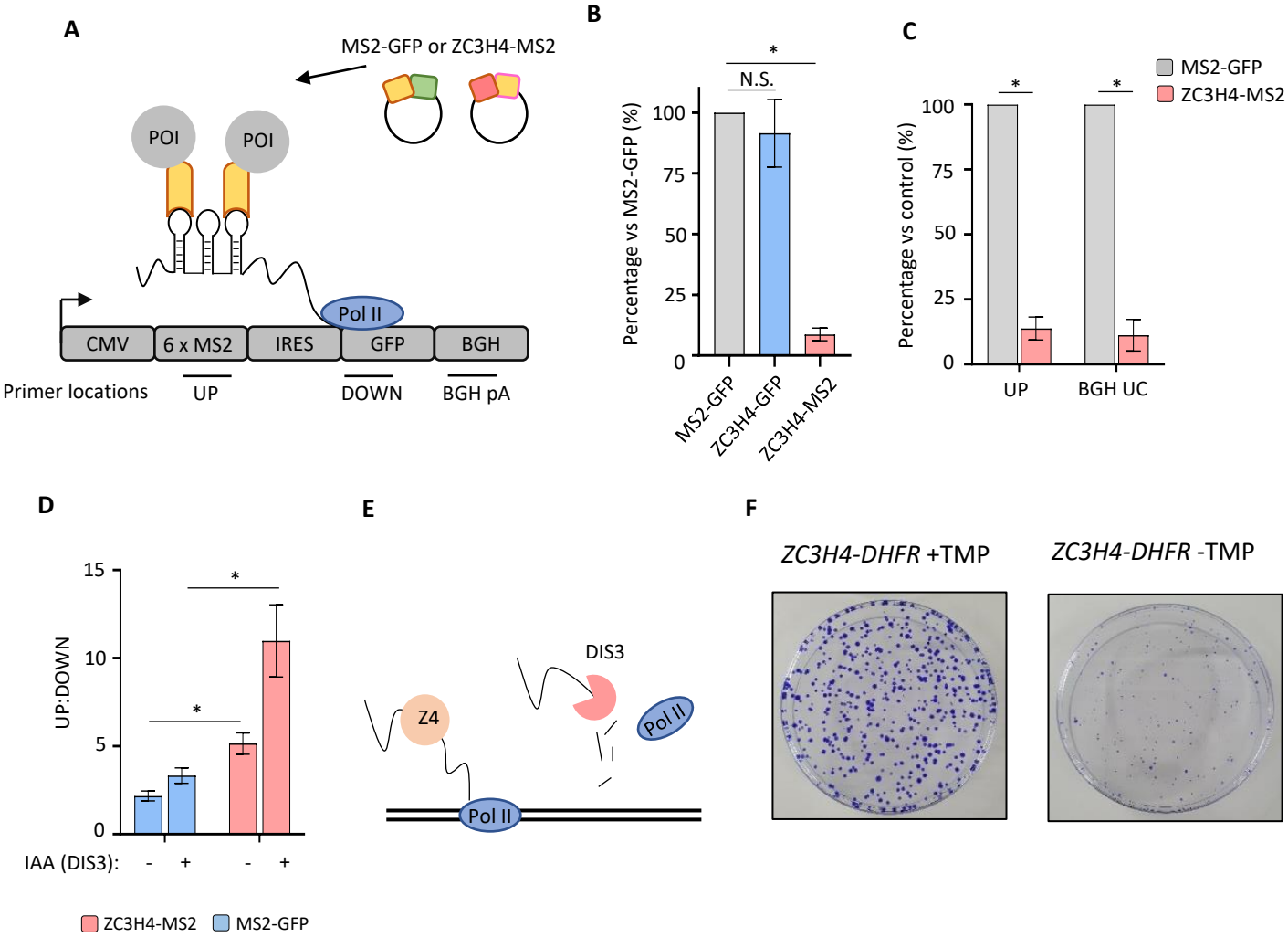
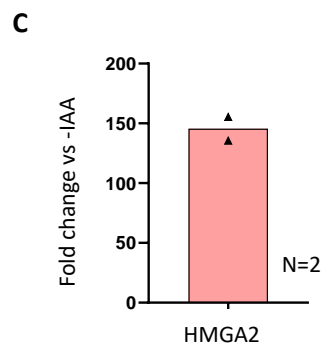
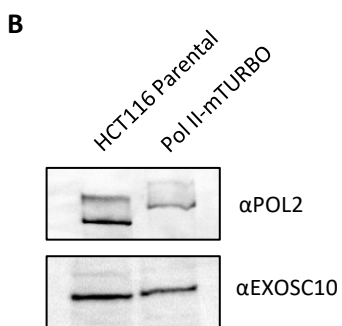
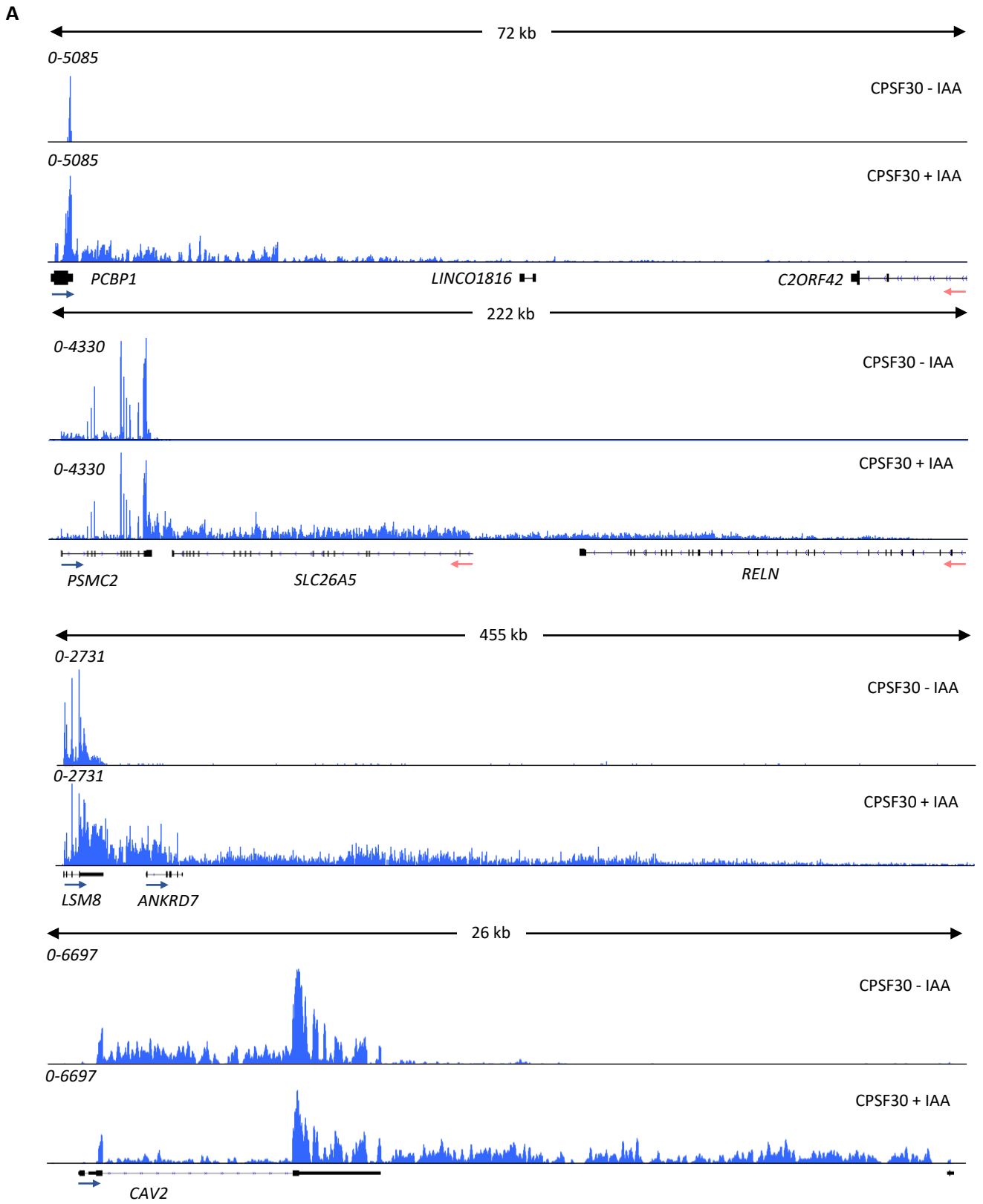
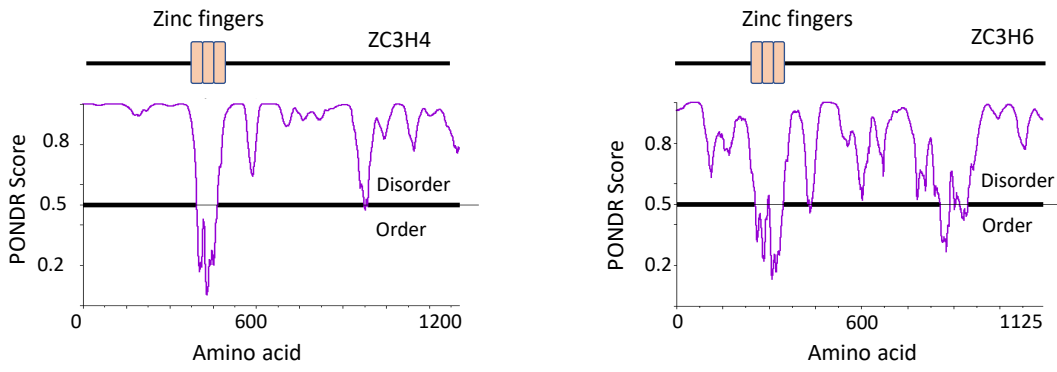


Figure 6

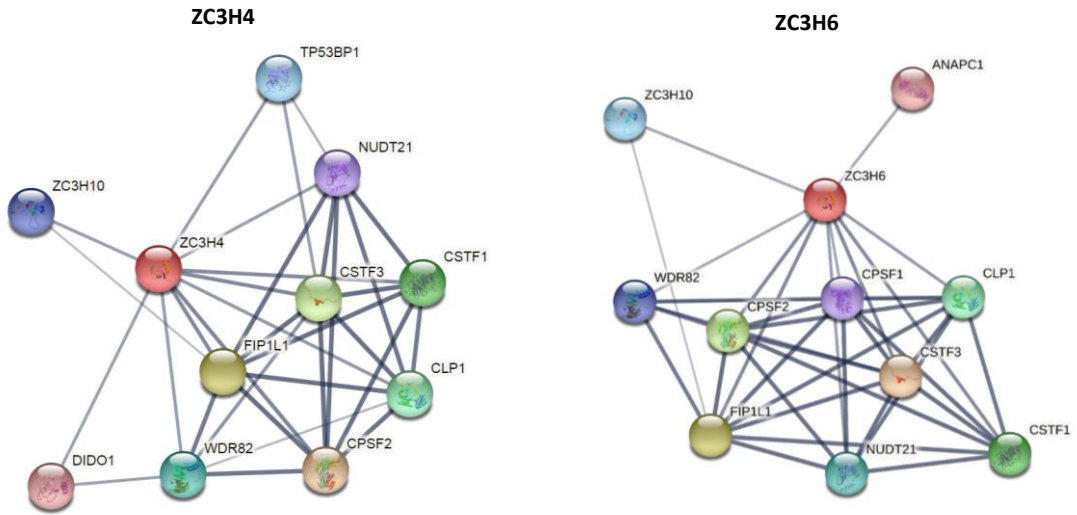




A



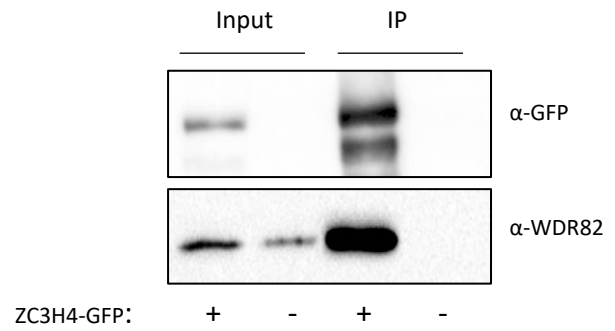
B



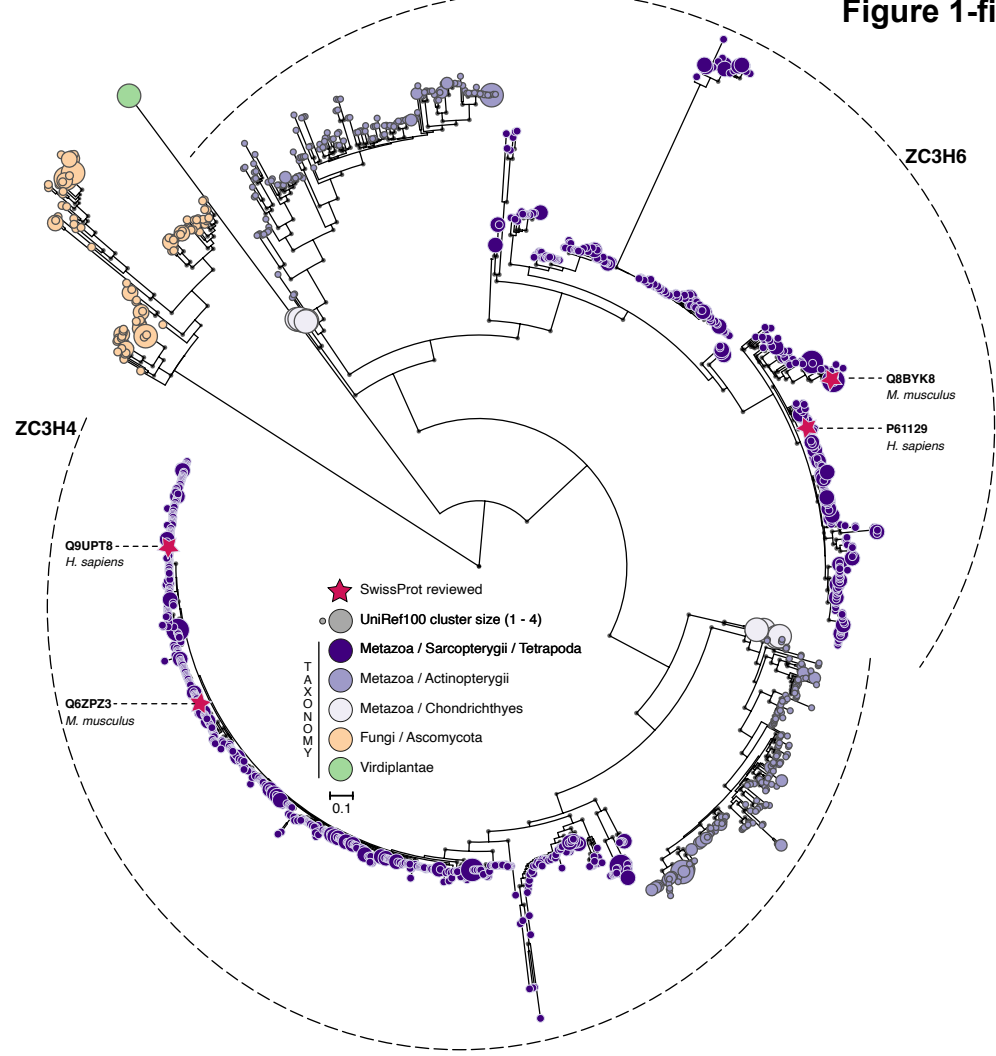
C

GO Biological Processes enriched among 19 identified proteins	No. of proteins	Adj p-value
RNA metabolic process	16	4.46E-06
gene expression	15	4.42E-04
mRNA processing	7	6.62E-04
cellular macromolecule metabolic process	17	4.58E-03
RNA splicing	6	6.44E-03
RNA biosynthetic process	11	9.45E-02

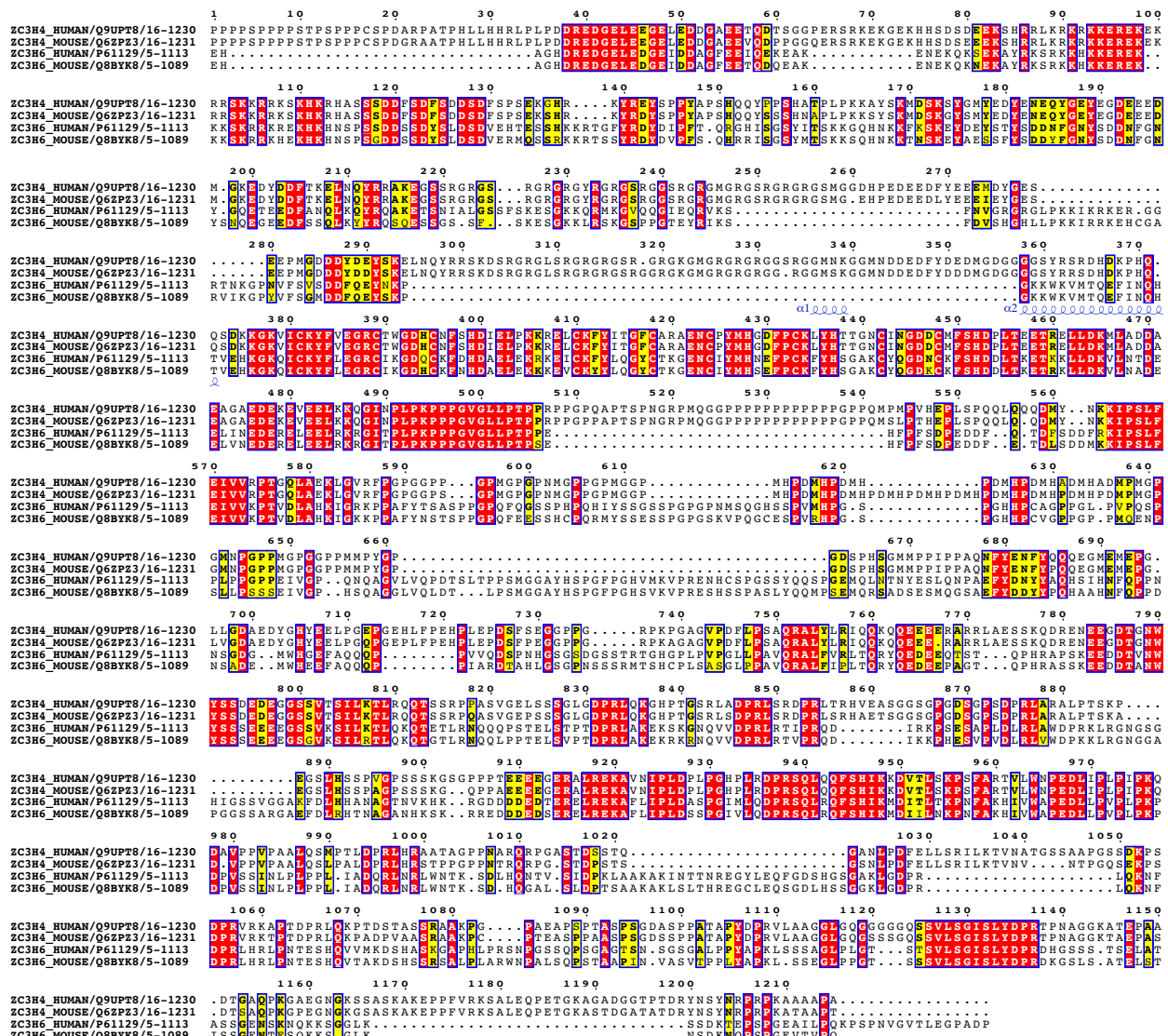
D

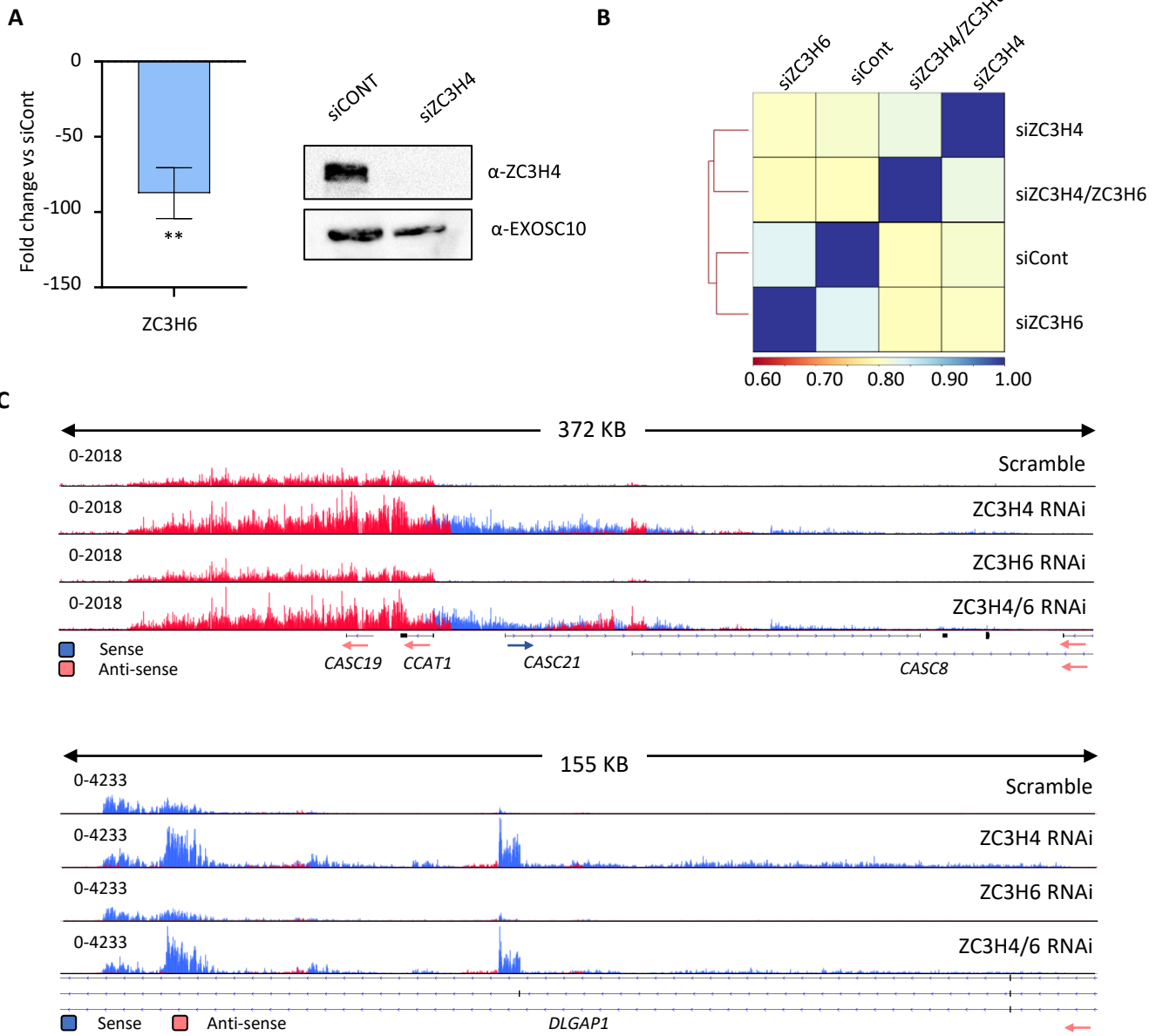


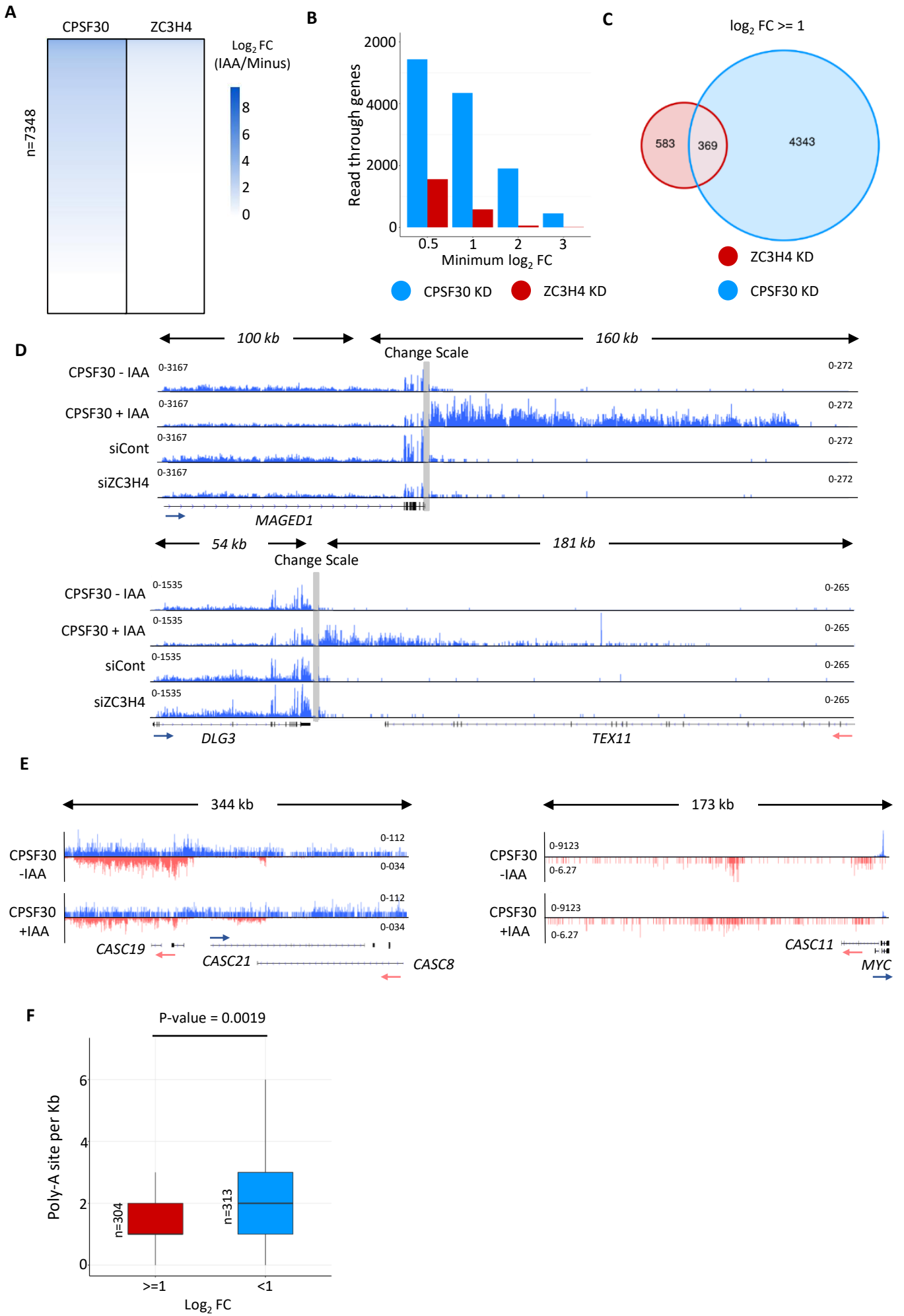
A



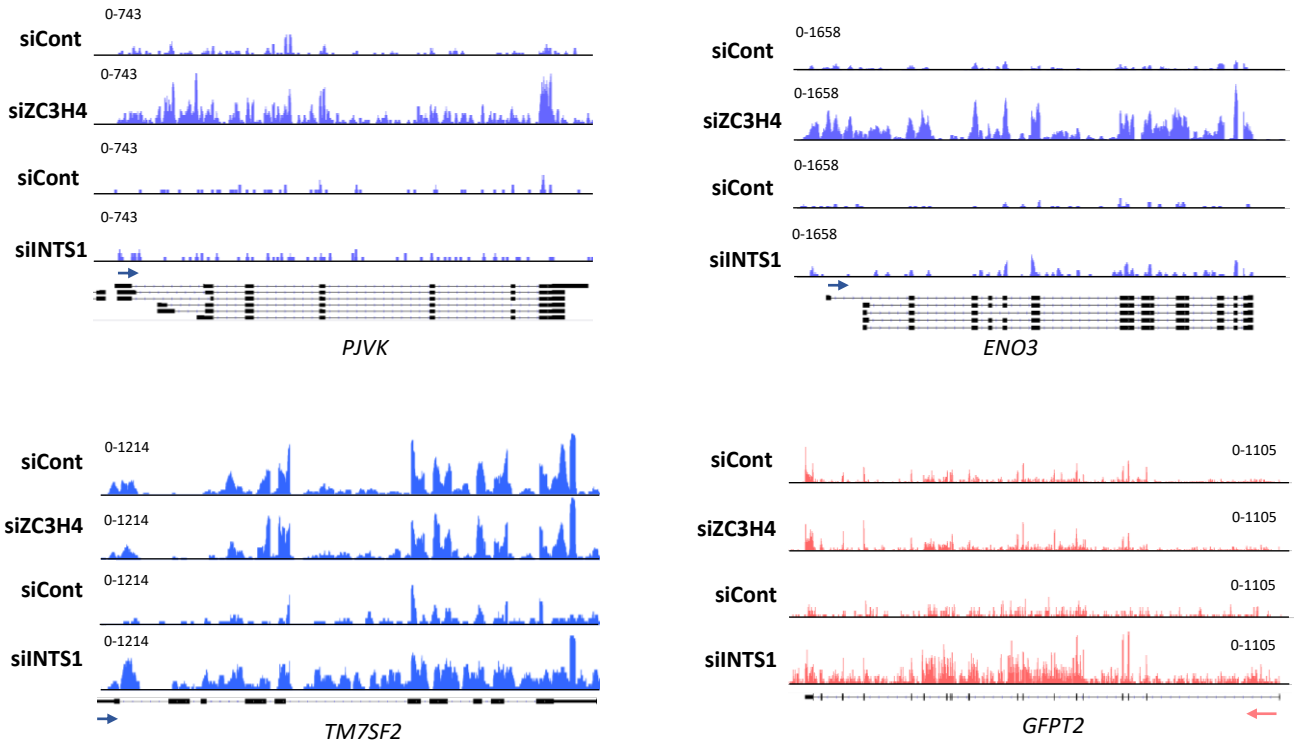
B



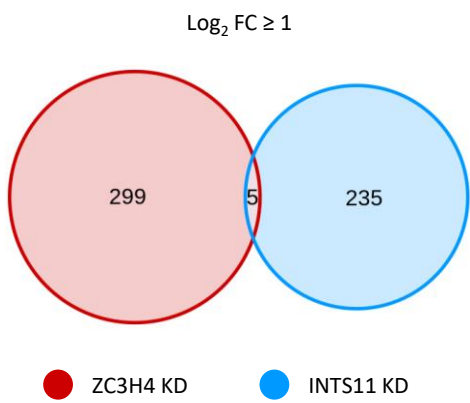




A

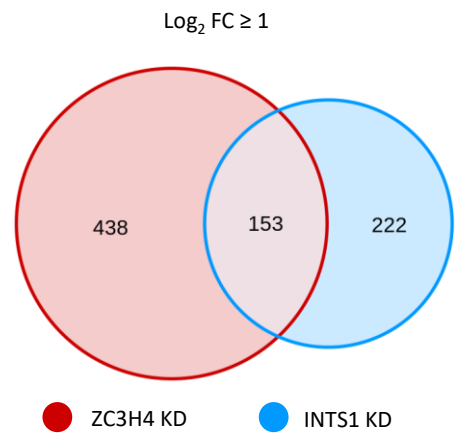


B



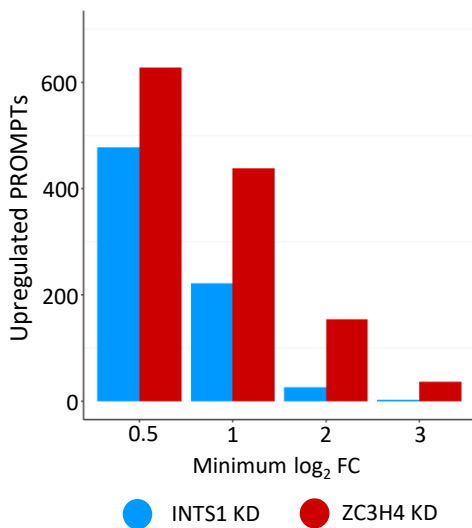
Upregulated mRNAs (HeLa)

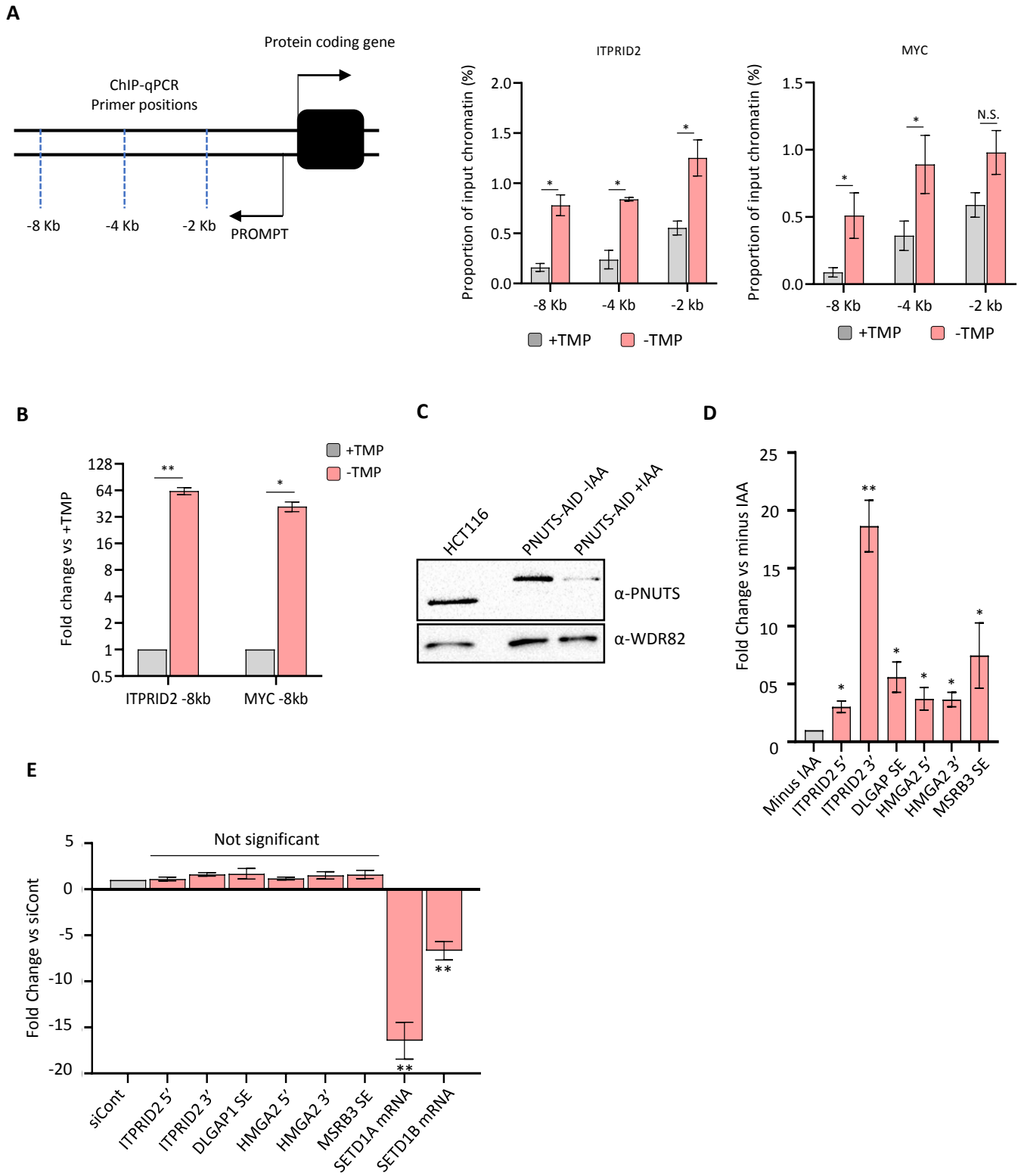
C



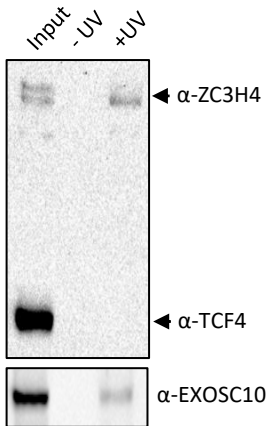
Upregulated PROMPTs (HCT116)

D

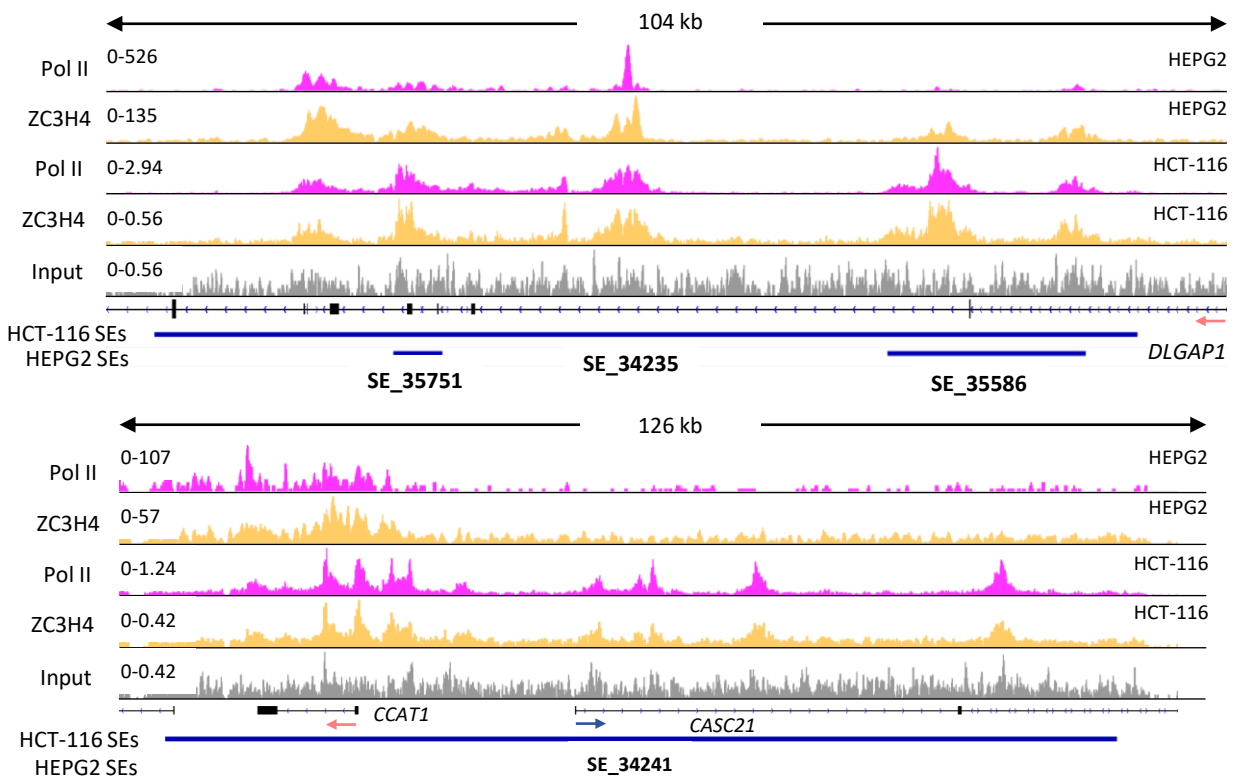




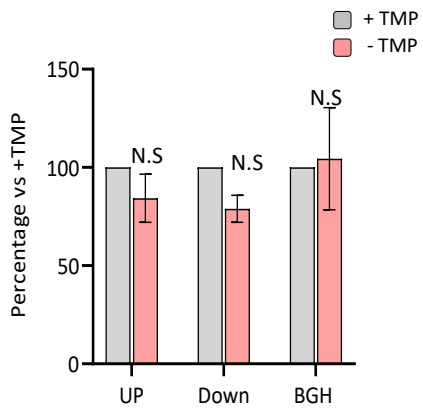
A



B



A



B

